Toward Systematic Understanding of Diversity of Electronic Properties in Low-Dimensional Molecular Solids

Hitoshi Seo*

Correlated Electron Research Center (CERC), AIST Tsukuba Central 4, Ibaraki 305-8562, Japan

Chisa Hotta

Department of Physics, Aoyama Gakuin University, Kanagawa 299-8558, Japan

Hidetoshi Fukuyama

International Frontier Center for Advanced Materials (IFCAM), IMR, Tohoku University, Miyagi 980-8577, Japan

Received March 17, 2004

Contents

* To whom correspondence should be addressed. Phone: +81-29-861-2986. Fax: +81-29-861-2586.

1. Introduction

Solids exhibit a variety of electronic properties such as elastic, magnetic, thermodynamic, transport properties, etc. Above all, the difference between insulating and metallic properties is most dramatic. Since the constituent atoms, if they are isolated, are neutral, the onset of metallic conduction which results from the motion of electrons between atomic sites is not trivial. This is, however, well explained in the textbook by the Bloch's band theory as being the realization of cases where the chemical potential is located within the energy band. On the other hand, if energy bands are fully occupied and the chemical potential is located within the band gap, an insulating state is realized which is called the band insulator. Such a difference can be understood also from the local point of view. In solids, the quantum tunneling of electrons is possible between different atomic sites. If the atomic orbital with the highest energy has one electron per orbital, metallic conduction is possible, whereas if two electrons are in the same orbital, the system as a whole becomes insulating as a result of Pauli principle. Such a kind of view for the onset of the conduction process is valid if the energy separation, Δ, between atomic orbitals is larger than the transfer integral, t, i.e., if the bands are well separated. In ordinary metals, however, this condition is generally not satisfied, and the resultant band structures are complicated, as seen in actual band structure calculations.

Besides such band insulators which are due to the basic principle of quantum mechanics, there are various mechanisms to make systems insulating even if the band theory predicts a metallic state. These

10.1021/cr030646k CCC: $48.50
Published on Web 10/23/2004

Hitoshi Seo was born in Osaka city, Japan, in 1972. He obtained his B.A. degree from University of Tokyo in 1995. In 2000, his Ph.D. was received from University of Tokyo, where he studied charge ordering phenomena in quasi-two-dimensional molecular solids, supervised by Hidetoshi Fukuyama. Subsequently he spent a year at the University of Tokyo in the group of Masao Ogata. In 2001 he joined the group of Naoto Nagaosa, the theory team of Correlated Electron Research Center (CERC), National Institute of Advanced Science and Technology in Tsukuba. He has proceeded in his work further aimed at new phenomena in strongly correlated electron systems, not only in molecular solids but also in transition metal oxides.

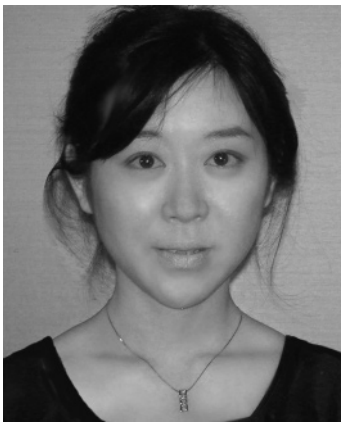

Chisa Hotta was born in Hiroshima in 1975. She obtained a B.A. degree in 1997 in the theoretical study on DCNQI systems and her Ph.D. in 2002 in the systematic study of the quasi-two-dimensional organic conductors both from the University of Tokyo. During these years she was engaged mainly in the study of the organic π–d systems supervised by Prof. Hidetoshi Fukuyama, and by Prof. Masao Ogata while she studied the ferromagnetism in CaB_6. She became a junior research associate in 2000 and then a Special Postdoctoral researcher from 2002 in RIKEN at the Condensed Molecular and Materials laboratory headed by Prof. Reizo Kato. Now in 2004, she is the research associate of Aoyama-Gakuin University under Prof. Kenn Kubo. She is now involved in the study of the magnetic and transport properties of strongly correlated electron systems.

are as follows:

1. Mott insulator in the case of a half-filled band.
2. Charge-ordered (CO) state in the case of commensurate fillings of the band.
3. Peierls insulators causing the bond alternation in one-dimensional (1D) systems such as in polyacetylenes, $(CH)_x$, which are the special case of instability due to the nesting of Fermi surface. These are essentially band insulators but doped carriers behave differently from those in the band insulators, i.e., like solitons.
4. Anderson localization due to disorder conceivable in any degree of band filling.

Hidetoshi Fukuyama is the Head of International Frontier Center for Advanced Materials (IFCAM) of the Institute of Materials Research (IMR), Tohoku University, in Sendai, Japan. He was born in Tokyo in 1942, graduated from the Physics Department of Tokyo University in 1965, and received his Ph.D. from Tokyo University in 1970. From 1970–1977, he was a post-doc and Associate Professor in the Physics Department of Tohoku University. During that period, he stayed in Division of Engineering and Applied Physics, Harvard University, from July, 1971 to March, 1973, and in Theory Group, Bell Telephone Laboratories, Murray Hill, New Jersey, from April, 1973 to March, 1974. From 1977–1992, he worked in the Institute of Solid State Physics (ISSP), Tokyo University, as an Associate Professor until 1984 and then as a Full Professor. From 1992–1999, he was Professor of Physics at Tokyo University and then moved to ISSP to be the Director until March, 2003. Since October, 2003, he has been at IFCAM.

These cases 1, 2, and 3 are schematically shown in Figure 1. The cases 1 and 2 are consequences of strong interaction between electrons (strong coupling effects), when the commensurability of the carrier number to the lattice is satisfied. On the other hand, in case 3, the geometry of the Fermi surface is an important factor; its nesting leads to charge-density-wave (CDW) or spin-density-wave (SDW) states, but the resultant state is not always an insulator unless when the system is purely 1D. There is a clear contrast between these two categories; the "real space" physics appears in the former, whereas in the latter the "momentum space" provides a better description.

During the past 30 years, there have been great efforts and then achievements in realizing conducting (metallic) states in molecular solids[1–3] as briefly

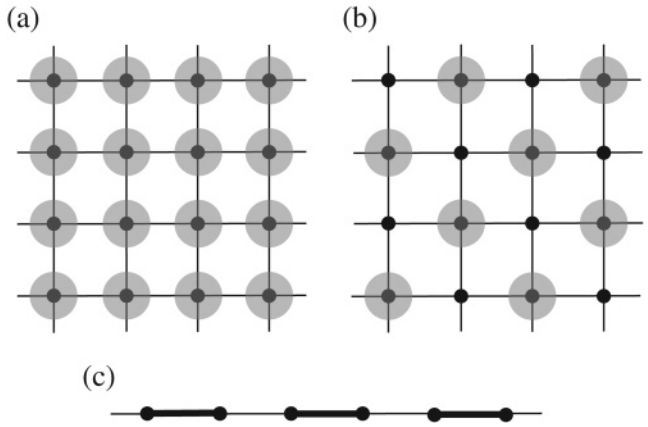

Figure 1. Schematic representations of (a) Mott insulator, (b) charge ordered state, and (c) Peierls insulator. Black dots, gray circles, and thick bonds represent lattice sites, localized electrons, and bond alternation, respectively.

Table 1. Representative Molecular Crystals Where Conducting (Metallic) States Are Realized[a]

compounds	electric property	phenomena
NMP-TCNQ	CT 1D semimetal or Mott insulator	1D AF
TTF-TCNQ	CT 1D semimetal	Peierls transition, CDW, gigantic conductivity peak, sliding conduction
$(CH)_x$	Peierls insulator (dimerization)	doping, carriers as in-gap states
TM_2X	CT metal	SDW, SC, AF, SP, CO, ferroelectricity
$DCNQI_2X$	CT metal	CO, Mott insulator, CO−Mott with Peierls
ET_2X	CT metal	Mott insulator, AF, SC, CO
$BETS_2X$	CT metal	SC, Mott insulator, field-induced SC
$TTM\text{-}TTP_2I_3$	1:1 half-filled, CT metal	Mott transition
$Ni(tmdt)_2$	single component metal	semimetal

[a] CT, AF, CDW, SDW, SC, SP, and CO stand for charge transfer, antiferromagnet, charge-density-wave, spin-density-wave, superconductor, spin-Peierls, and charge order, respectively.

categorized in Table 1. The strategy behind has been to combine different kinds of molecules and/or ions and generate charge transfer between them when crystallized. This is because molecules alone have a closed shell, and therefore, crystals consisting of a single kind of molecule are usually band insulators,[4] in accordance with the local picture above. In the early stage of the research, compounds consisting of 1:1 composition between two kind of molecules *A* and *B*, the "*AB* compounds", were mainly synthesized. Later on, 2:1 compounds, i.e., the "A_2B compounds", were found to be more suitable for realizing conducting systems. Furthermore, besides simple metallic states, the A_2B compounds show rich physical properties such as the various insulating states pointed out above.

For an understanding of these molecular solids, the local approach explained above is very suited, since the condition $\Delta > t$ is usually satisfied where the roles of the atomic orbitals in that consideration can be replaced by the molecular orbitals. This is because of a larger size of molecules compared to that of atoms leading to small local amplitude of wave function and hence to a smaller t between them. Also, a relatively larger distance between molecules because of the van der Waals bonding leads to smaller t, compared to that in usual compounds composed of atoms with stronger bonding. In such cases, either HOMO (highest occupied molecular orbital) or LUMO (lowest unoccupied molecular orbital), termed as frontier orbitals by Fukui,[5] are the determining factors of the electronic properties in molecular solids. This can be viewed as an extension of the idea of the frontier orbital theory for chemical reaction of molecules to molecular solids. The notable feature of molecular solids is that t between this HOMO or LUMO always have strong anisotropy. This anisotropy reflects particular shapes of molecules (i.e., planer in most cases) and leads to various band structures and then to electronic properties in systems with different arrangement of molecules in the unit cell.

Our aim in this review is to search for a possible systematic theoretical understanding of particular electronic properties of the conducting A_2B compounds based on the frontier orbitals, HOMO and LUMO. The main interests will be (1) How are the metallic states realized? and (2) What kinds of ground states are expected in each case? The basic Hamiltonian to examine this problem will be the tight-binding model based on either HOMO or LUMO of relevant molecules (e.g., referring to the results of the extended Hückel calculation[6,7]) together with Coulomb interaction not only within the same site, U, but also between neighboring sites, V_{ij}, as well. This is called the extended Hubbard model, represented as

$$H = \sum_{\langle ij \rangle}\sum_{\sigma}(t_{ij}c_{i\sigma}^{\dagger}c_{j\sigma} + h.c.) + \sum_{i}Un_{i\uparrow}n_{i\downarrow} + \sum_{\langle ij \rangle}V_{ij}n_in_j \quad (1)$$

where $\langle ij \rangle$ denotes the pair of the lattice sites i and j and σ is the spin index which takes $\uparrow$ or $\downarrow$. The transfer integrals, t_{ij}, take full account of the anisotropy resulting from the particular spatial extent of molecular orbitals of HOMO or LUMO. The validity of such tight-binding models has been confirmed by the finding that its calculated results agree with the observed Fermi surfaces in various compounds. Particularly, the LDA band structure calculations taking into account of about 90 atoms in the unit cell for $DCNQI_2X$ (X = Cu, Li, Ag) by Miyazaki et al.[8,9] is noteworthy. Their results based on such detailed calculations are in accordance with the de Haas-van Alphen experiment in $(DMe\text{-}DCNQI)_2Cu$[10] and also with those based on the tight-binding approximation by use of the overlap integrals of the extended Hückel calculation.[11] Although there is no general guarantee of the validity to apply the extended Hückel scheme, it will be ascertained a posteriori, and we will assume it in this review.

The electron−electron Coulomb repulsion described by the last two terms in eq 1 is important to understand the diversity in the electronic properties of molecular solids. A theoretical attempt to study such effects in conducting A_2B systems in a systematic way was first done by Kino and Fukuyama[12] by taking the anisotropy of t_{ij} into full account. They considered the Hubbard model ($V_{ij} = 0$) and treated the on-site U term within standard mean-field approximation, but adopting the values of t_{ij} from the extended Hückel scheme mentioned above. This study on ET_2X (ET = BEDT-TTF) as a typical example opened a path to pursue an understanding of the physical properties of the conducting A_2B systems. It made clear how to deal with apparently complicated molecular solids in a transparent way

similarly to the conventional solids on a general ground; the molecular solids can be studied based on molecular orbitals compared to atomic orbitals in conventional solids.

The extended Hubbard model represented by eq 1 can be commonly applied to a broad range of compounds, but the actual values of parameters differ from compound to compound. For example, the "on-molecule" U varies to some extent depending on the molecule (see the following sections for specific cases) but is usually considered to take the same value for the same molecule and is typically of the order of bandwidth, ~1 eV.[2] On the other hand, t_{ij} is more sensitive to the molecular arrangements as has already been pointed out, and as for V_{ij}, the point charge relation $V_{ij} \propto 1/r_{ij}$ approximately holds where r_{ij} is the distance between the center of two molecules i and j.[14] (Notable here is that transfer integrals t_{ij} decay exponentially as a function of r_{ij}.[14]) The consideration of this Coulombic V_{ij} term in eq 1 is now understood to be crucial for CO states[15] which are of recent interest, and we put special emphasis on it in this review. As a matter of fact, the value of V_{ij} between neighboring molecules can be as large as ~50% of U estimated in some compounds.[16,17] The effects of electron−phonon interactions, not included in eq 1, will be examined separately. More general aspects of conducting molecular solids can be found elsewhere.[1−3,18,19]

2. Characteristic Features of Conducting Molecular Solids

As we have introduced in the previous section, charge transfer is important for realizing conducting molecular solids. Depending on the degree of the charge transfer and on whether the resulting molecular states are in the closed shell or not, different types of electronic states emerge. We will first summarize briefly such electronic states in representative conducting AB compounds and then introduce typical features of the A_2B compounds in short.

2.1. Brief Summary of *AB* Compounds

As seen in Table 1, there are examples of AB compounds where a metallic state is stabilized. One of the compounds attracting interest in early days is NMP-TCNQ, where the amount of charge transfer was first considered to be one from NMP to TCNQ, resulting in closed shell of NMP^+ and then half-filled band of $TCNQ^-$. The onset of a gradual metal−insulator (MI) transition seen in the temperature dependence of resisitivity at around 200 K, below which the spin susceptibility has strong dependence on temperature, was interpreted to be due to the Mott transition.[20] On the other hand, X-ray scattering measurements suggest that the amount of charge transfer is 2/3 and that the insulating behavior is then to be due to the Peierls transition.[21] Possible effects of positional disorder in the ethylene group of the asymmetric NMP molecules should be taken into account for the full understanding of the electronic properties of this compound.[22]

In the case of TTF-TCNQ and its analogues, which have been attracting much interest since their synthesis,[18,19] the amount of charge transfer is fractional and is close to 2/3, resulting in the contribution to the transport properties from both TTF and TCNQ chains. The large peak in conductivity just above 50 K was first considered to be due to the fluctuation of a superconducting (SC) state[23] but now understood as due to the collective (phason) transport associated with the Peierls transition.[18,19] The Peierls transition leads to the CDW ground state, which is found in many different kinds of compounds.[24]

There is also a recent example, $(TTM\text{-}TTP)I_3$,[25,26] with the closed shell of $(I_3)^-$ and half-filled band of $TTM\text{-}TTP^+$. The MI transition-like large change of resistivity around 150 K at ambient pressure is attributed to the Mott transition. It is to be noted that the spin susceptibility below this characteristic temperature is seen to be suppressed in contrast to the case of NMP-TCNQ and is argued as the onset of the spin-Peierls (SP) state. In fact, the X-ray observation of the superlattice below this characteristic temperature suggests the formation of dimers between the spins $S = 1/2$ on TTM-TTP due to lattice distortions.

2.2. Representative Features of A_2B Compounds

There are many examples of this category with either a 1D or two-dimensional (2D) array of molecules, where B molecules are fully charged either as a -1 or $+1$ forming closed shell. Therefore, the average valence of A molecules is either $+1/2$ or $-1/2$ and then the energy bands formed by HOMO or LUMO of A molecules are quarter-filled in terms of holes or electrons, respectively, if the A sites are equivalent, as shown in Figure 2 (in this section only the case of B^+ and then Figure 2b will be considered, since the same physical consideration can be applied to both cases).

In such A_2B compounds, most typically two limiting cases can be considered in the presence of strong correlation depending on the degree of dimerization as schematically shown in Figure 3 for 1D systems.[13,27] In the absence of dimerization, electrons will favor to stay apart from each other if the kinetic energy characterized by the bandwidth is relatively small compared to the Coulomb interaction. This results in nonuniform distribution of charge density between molecules, i.e., charge disproportionation (CD). In the quarter-filled case the charge will occupy

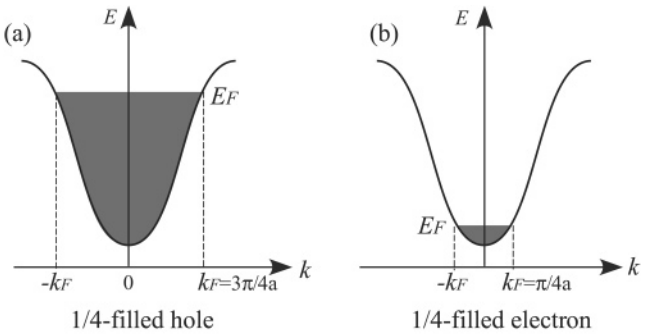

Figure 2. Schematic representations of (a) 3/4-filled and (b) quarter-filled bands in one-dimensional case. E_F, k_F, and a represent the Fermi energy, the Fermi momentum and the lattice constant, respectively.

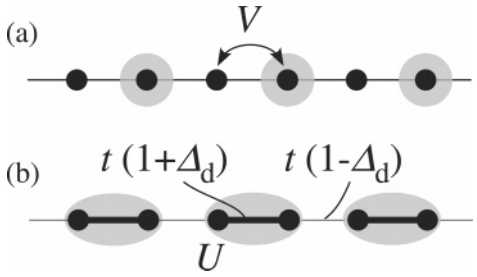

Figure 3. Schematic representations of two limiting cases in one-dimensional quarter-filled system: (a) the charge ordered state and (b) the dimer-Mott insulating state. Black dots and gray circles represent the lattice sites and the localized carriers, respectively.

every other site as shown in Figure 3a; i.e., a CO state is realized, which is a long-range-ordered state of CD. It should be emphasized that the intersite Coulomb interaction, V_{ij}, plays crucial roles for this kind of CO state which can be considered as a Wigner crystal on lattices.[28] On the other hand, in the presence of strong dimerization, a single electron will occupy the bonding state of each dimer as shown in Figure 3b leading to an effectively half-filled band and then to the Mott insulating state due to the effect of U, which we call a dimer-Mott (DM) state. In this state, the charge distribution is uniform among molecules.

In the actual compounds, there are many situations between these two limiting cases and the resultant electronic state is not so simple. This is because the molecular solids have moderate value of Coulomb interactions comparable with the kinetic energy represented by the bandwidth, as mentioned above. The reality lies between these limiting cases and the ground states actually realized depends on the band structure of each material, which is affected by the anisotropy of t_{ij} as we will see later.

In the limiting case of the CO state, there should be a localized spin $S = 1/2$ on every other "charge-rich" site. In the DM state, on the other hand, the localized spin $S = 1/2$ is on each dimer. For both cases, the effective Heisenberg exchange coupling between these spins depends on the transfer integrals between sites/dimers where the electrons are localized, due to the superexchange process. For example, both states in a and b of Figure 3 are described by the 1D Heisenberg models with uniform exchange coupling, J.

3. Experimental Overview of A_2B Compounds

There is a variety in A_2B compounds, and their diverse electronic properties have been revealed by experimental studies. In view of the possible characteristic features theoretically expected in the limiting cases of A_2B compounds explained above, various systems actually synthesized will be categorized and their properties be summarized in the following, so that one can see the characteristic features of each family.

3.1. $DCNQI_2X$

The structure of $DCNQI_2X$ is schematically shown in Figure 4, where DCNQI is a shorthand for R_1R_2-

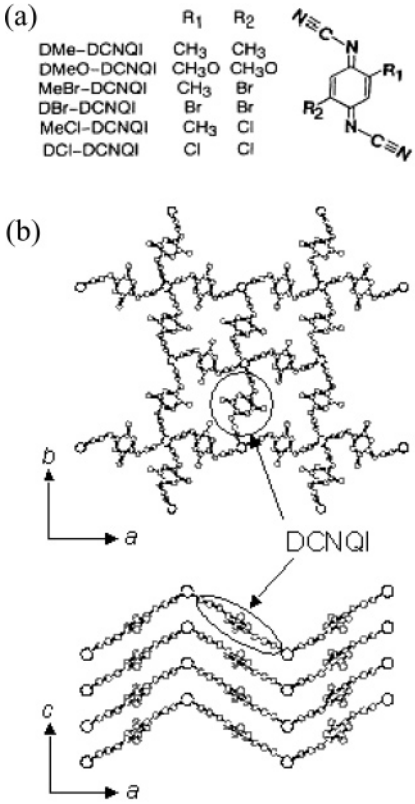

Figure 4. (a) DCNQI molecule with examples of substituents, R_1 and R_2 (Reprinted with permission from ref 32. Copyright 1993 The American Physical Society) and (b) crystal structure of $DCNQI_2X$.

DCNQI molecule.[29] As seen in Figure 4a, DCNQI can be chemically modified by varying the groups R_1 and R_2 with Cl, Br, I, CH_3 (= Me), CH_3O, etc. In the following, we omit R_1R_2- and write DCNQI in general but denote them explicitly when necessary. In the cases of X = Li and Ag, the valence of X is +1 and then the π-band of DCNQI is quarter-filled, whereas the average valence in the case of X = Cu is close to +4/3, which is a particular case. As a result, their physical properties are very different although these are all isostructural.

3.1.1. X = Li, Ag

The temperature dependences of electrical resistivity, ρ, and magnetic susceptibility, χ, of DMe-$DCNQI_2$-Ag and DI-$DCNQI_2$Ag, which show typical behavior of this family, are shown in Figure 5.[30] These compounds are metallic or semiconducting at room temperature and turn gradually into an insulating state upon cooling. Their data of χ show a characteristic behavior expected for a low-dimensional localized spin system, and at low temperature, a magnetic phase transition takes place to either an antiferromagnetic (AF) state or a nonmagnetic SP state.

3.1.2. X = Cu

This family has been intensively studied because of their three-dimensional nature which is apparently unexpected[31] and a dramatic MI transition of first-order nature with sudden jumps in ρ of several orders

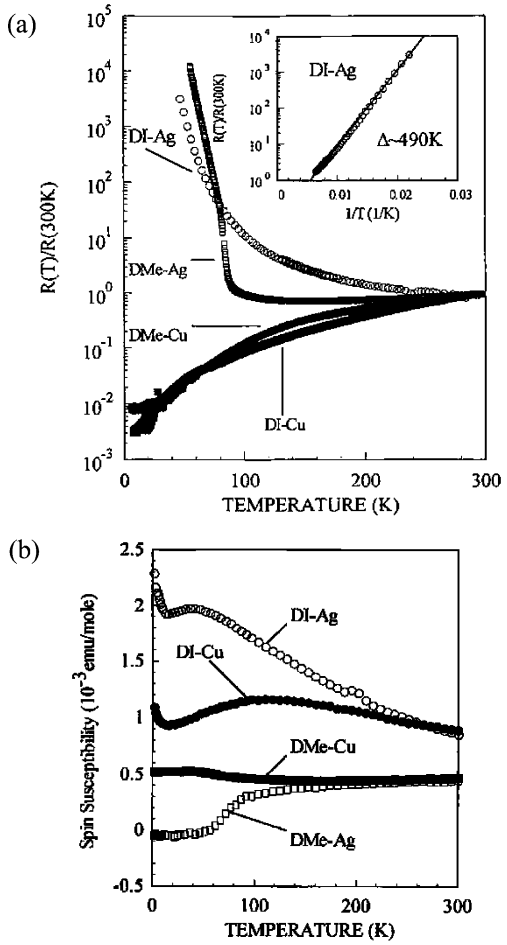

Figure 5. (a) Electrical resistivity, ρ, and (b) magnetic susceptibility, χ, of R_1R_2-DCNQI$_2X$ with $R_1 = R_2 =$ I, Me and $X =$ Ag, Cu in the metallic phases. (Reprinted with permission from ref 30. Copyright 1996 The American Physical Society.)

of magnitude.[11] Their phase diagram on the plane of pressure and temperature is summarized as in Figure 6.[32] Each compound with different R_1 and R_2 is located in a certain position along the transverse axis, and by applying the external pressure to each compound, their behavior changes continuously to that of the other compounds with smaller unit cell sizes. Therefore, substituting the molecule without changing the structure can be considered as applying "chemical pressure",[33] and this concept generally holds for the phase diagrams of many molecular solids as we will see below. In Figure 6, one can see that the MI phase boundary is very sensitive to these factors, and a notable point is the existence of a re-entrant behavior of the MI transition as a function of temperature in a very narrow range of effective pressure.

In Figure 7, the temperature dependences of ρ and χ for members of DCNQI$_2$Cu near the MI phase boundary are shown.[34] In the metallic phase, χ has a weak temperature dependence similar to Pauli paramagnetic susceptibility, whereas in the insulating phase, on the other hand, χ shows a Curie-like behavior. In the latter, if one assumes the existence of localized spin of $S = 1/2$ on the Cu chains, the population of spin corresponds to 1/3 of the Cu sites.

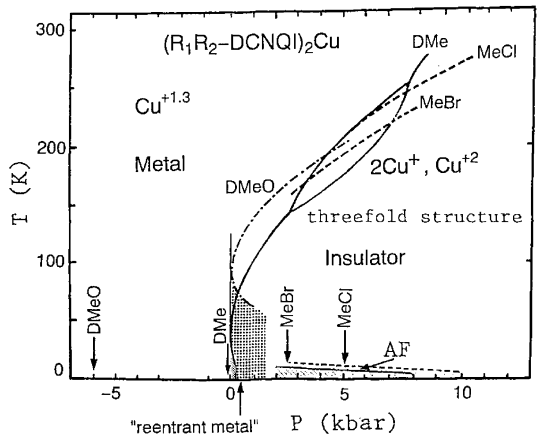

Figure 6. Experimental phase diagram of DCNQI$_2$Cu. The arrows show the location for the ambient pressure properties of different substituent groups shown in Figure 4(a), indicated as R_1R_2. The shaded and the dotted area represent the re-entrant metallic and the antiferromagnetic (AF) state, respectively. (Reprinted with permission from ref 32. Copyright 1993 The American Physical Society.)

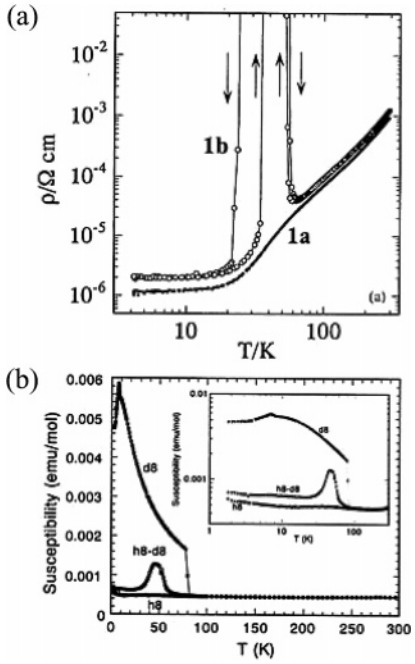

Figure 7. (a) Electrical resistivity, ρ, and (b) magnetic susceptibility, χ, of DMe-DCNQI$_2$Cu tuned by substituting isotope atoms. In (a), 1a and 1b are data for unsubstituted salts and those for salts with carbon sites in cyano group substituted by ^{13}C, and in (b), h8, d8, and d8−h8 are data for undeutrated salts, fully deutrated salt (i.e., all H → D), and their 4:6 alloyed salts, respectively. (Reprinted with permission from ref 34. Copyright 1993 Pergamon Press Ltd, and 1995 Elsevier Science S.A.)

Hence, this insulating phase will be characterized by a particular localization of charge on Cu sites as (Cu^+ Cu^+ Cu^{2+}), which is actually confirmed experimentally.[35] At the same time, a 3-fold periodic lattice distortion occurs on the DCNQI chain.[11] It is mentioned that, in the cases of R_1 and R_2 containing iodine, the external pressure leads to a series of transitions from the insulating state with 3-fold periodicity to another metallic state and then to an insulating state again at higher pressure,[36] as shown in Figure 8.

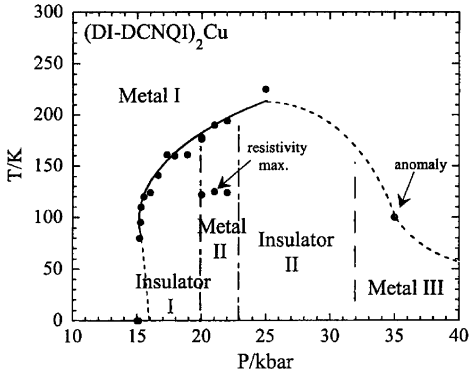

Figure 8. Experimental phase diagram of DI-DCNQI$_2$Cu based on resistivity measurements. The region "Insulator I" is where the insulating state with 3-fold periodicity is stabilized[36] (courtesy of Y. Kashimura). The detailed properties of other phases, "Insulator II", "Metal I", and "Metal II", are not yet known.

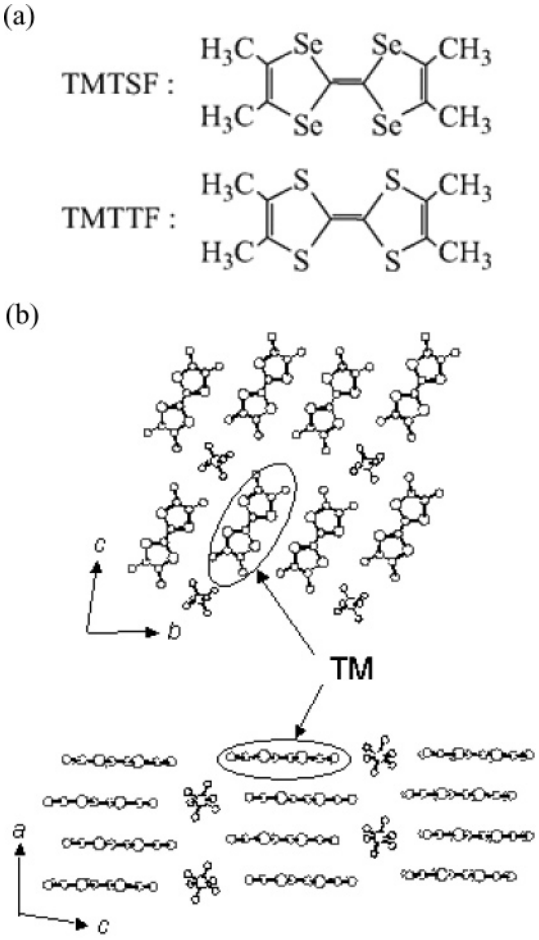

Figure 9. (a) TMTSF and TMTTF molecules and (b) crystal structure of TM$_2X$.

3.2. TM$_2X$

The TMTCF$_2X$ system, where TMTCF (abbreviated as TM) = TMTSF or TMTTF molecules, shown in Figure 9a, has been extensively studied for more than 20 years since the discovery of SC in TMTSF$_2$PF$_6$ in 1979.[37] The crystal structure of TM$_2X$ is shown in Figure 9b, where X is a closed shell anion, X^-, so that the π band of TM molecules is 3/4-filled. Jérome and co-workers summarized their physical properties in a phase diagram on the plane of temperature and

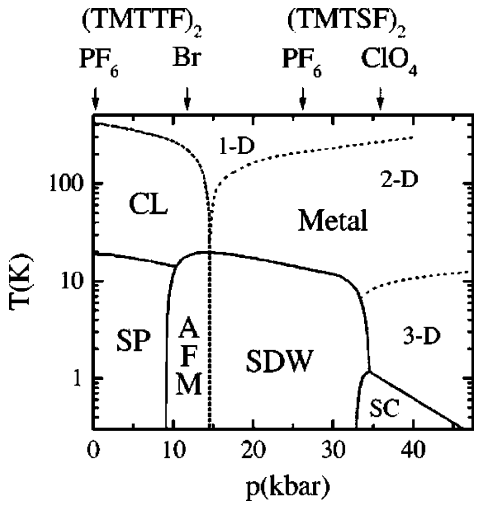

Figure 10. Jérome's experimental phase diagram of TM$_2X$. CL, SP, AFM, SDW, and SC stand for charge localization, spin-Peierls, antiferromagnet, spin-density-wave, and superconductor, respectively. Note that the CL phase is defined as below the temperature where the resistivity shows a miminum; this is not a phase transition but a crossover temperature. (Reprinted with permission from ref 42. Copyright 2000 The American Physical Society.)

(effective) pressure as shown in Figure 10.[38] The difference between TMTSF and TMTTF is the relatively widespread wave function of the former due to the larger Se orbital than S; this leads to larger transfer integrals in TMTSF compounds especially in the direction transverse to the TM columns[7,39] and to larger value of U in the TMTTF, i.e., $U_{\mathrm{TMTTF}} > U_{\mathrm{TMTSF}}$.[16,17] Therefore, it is natural that in Jérome's phase diagram TMTTF$_2X$ is mainly on the left (low pressure) side while TMTSF$_2X$ is on the right (high pressure) side; the former is expected to show a stronger tendency toward insulating states due to electron correlation as discussed in section 2.2, since the pressure increase in the horizontal axis increases the transfer integrals reducing the correlation effects.

The electrical resistivity, ρ, of each compound exhibits characteristic temperature dependence as shown in Figure 11.[38,40] In the case of TMTSF$_2$PF$_6$, a MI transition is seen in ρ at around 10−20 K, which is the onset temperature of the SDW state. The anisotropic behavior of the magnetic susceptibility, χ, is found there with a well-defined kink expected from the general understanding of the ordering of spin moments.[38]

TMTTF compounds, by contrast, in fact show more insulating characters. An MI crossover behavior is seen in ρ with a minimum at around T_ρ = 100−200 K.[38,40] However, until recently, there have been no physical quantities which point to the existence of a phase transition around these minima, whereas a kink in the thermopower and a maximum in the dielectric constant is found at somewhat lower temperatures; these features have been called the "structureless phase transition".[41] Through this crossover region, χ does not show any anomaly and behaves as that of a localized spin system, whereas magnetic phase transition to either AF or SP states occurs at well below this region.[38,42] These behaviors of ρ and

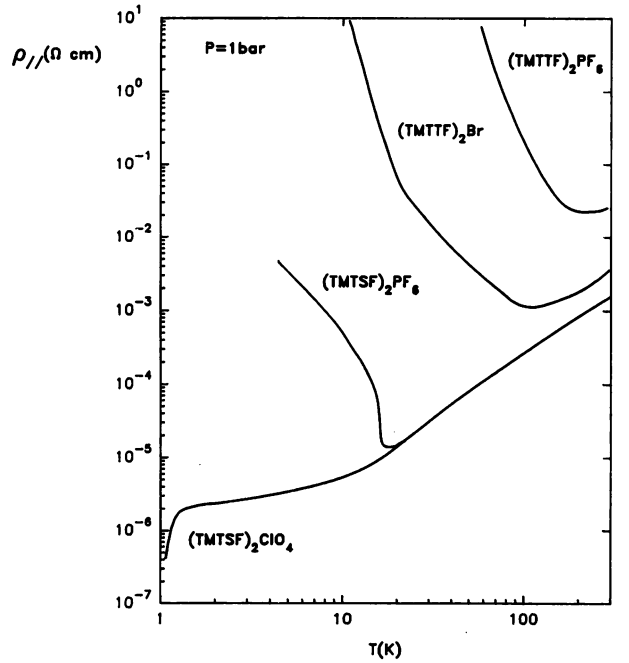

Figure 11. Electrical resistivity, ρ of several members of TM_2X. (Reprinted with permission from ref 40. Copyright 1993 EDP Sciences.)

χ are similar to those in $DCNQI_2X$ with X = Li, Ag, as seen in section 3.1.1.

3.3. Two-Dimensional Systems: ET_2X and $BETS_2X$

Interesting A_2B compounds with 2D nature were realized in early 1980s following the successful synthesis of the BEDT-TTF (abbreviated as ET) molecules, which is shown in Figure 12a.[2] With the amount of charge transfer as X^-, $ET^{1/2+}$ form 2D planes of 3/4-filled electronic systems on the average. There exist many polytypes in this family categorized by the Greek letters, α, β, κ, θ, etc.,[43] representing

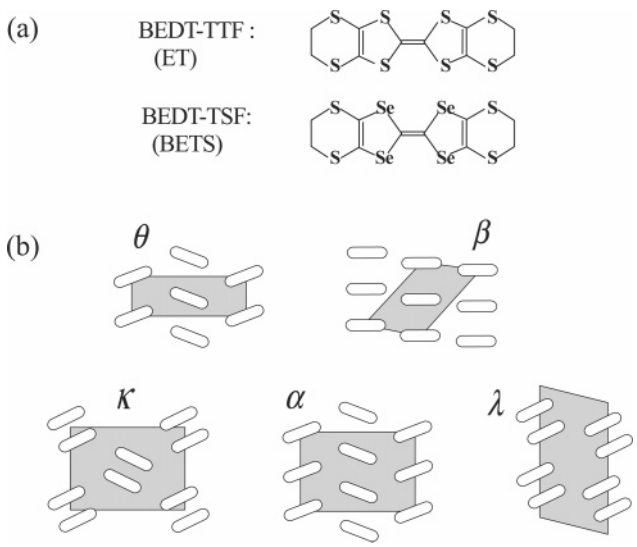

Figure 12. (a) ET and BETS molecules and (b) schematic representation of spatial arrangements of these molecules in the 2D plane for different polytypes, where the ellipses and the gray area represent the molecules and the unit cells, respectively.

different spatial arrangements of ET molecules which show different electronic properties. Here, we will focus on the extensively studied polytypes with either two or four molecules in the unit cell; the representative examples of the former are θ- and β-types and those of the latter are κ-, λ-, and α-types. The spatial arrangements of the molecules in the unit cell of these polytypes are schematically shown in Figure 12b.

If the energy bands are not strongly dispersive and are separated energetically with each other, the band theory for θ- and β-type compounds would predict that the Fermi level falls in the center of the upper band which will then be half-filled, and simple metallic states are expected. On the other hand, in κ-, λ-, and α-type compounds with four ET's in the unit cell the Fermi level would be located within the gap between the highest and the second bands, leading to band insulators. However, the electronic properties actually observed are truly diverse as will be introduced in the following.

There are compounds consisting of derivatives of the ET molecule, for example its selenium variants such as BETS (= BEDT-TSF)[44,45] shown in Figure 12a, and its oxygen variants such as BO (= BEDO-TTF).[2] In this review, we concentrate on ET- and BETS-based materials in which cases many systematic experimental studies have been carried out so far. The BETS molecule has a HOMO more widely spread compared to that of the ET molecule,[44] and then the value of U for BETS, U_{BETS}, is expected to be smaller than that for ET, U_{ET}.[45] Therefore, similarly to the case of TMTTF and TMTSF explained above in section 3.2, the ET salts usually show stronger tendency toward insulating states due to electron correlation than the BETS salts, as we will see in the following for each polytype. Another characteristic feature of the BETS compounds compared to the ET compounds is that there are compounds which contains magnetic anions, $X = FeY_4$ (Y = Cl, Br, etc.) with Fe^{3+} (S=5/2) interacting with the BETS π-conducting plane,[46] as we will see in sections 3.3.3 and 3.3.4.

3.3.1. θ-Type

The experimental phase diagram of θ-ET_2X is summarized by Mori et al. as shown in Figure 13, characterized by the dihedral angle, ϕ, defined as the angle between the molecules in adjacent columns.[47] (In ref 47, this is defined as θ but we use ϕ instead in this paper to avoid confusion.)

In the region of large ϕ, the ground state is insulating and there exists a sharp increase of ρ (MI transition) below some characteristic temperatures at around 100 K, as shown in Figure 14a, where a structural phase transition is concurrently observed.[47] The temperature dependence of χ, which is shown in Figure 14b,[47] is rather smooth through these temperatures behaving similarly to a low-dimensional localized spin system, and a crossover to a spin gapped behavior is seen below around 10 K.

On the other hand, in the region of smaller ϕ, such a sharp transition is absent but with decreasing temperature, ρ gradually increases below around 50

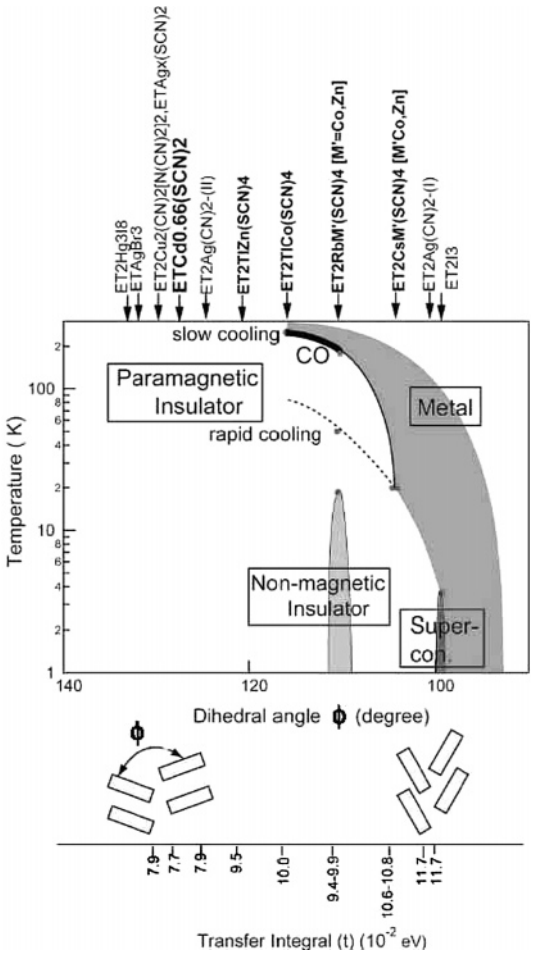

Figure 13. Mori's experimental phase diagram of θ-ET_2X classified by the dihedral angle, ϕ[47] (courtesy of H. Mori).

K, whereas χ also shows an increase from similar temperatures with a Curie-like behavior. When ϕ is further decreased, a normal metallic state is stabilized, where there exists the only material in this family showing a SC ground state, θ-ET_2I_3. θ-$BETS_2X$ are located in this phase diagram in the region of small ϕ,[48] consistent with $U_{BETS} < U_{ET}$.

3.3.2. β-Type

The first SC at ambient pressure in ET-based materials has been found in this polytype;[2,49] β-ET_2I_3 is known for having two different SC phases at $T_c \sim$ 1.5 and 8 K, respectively, and other β-ET_2X materials with $X = IBr_2$ and AuI_2 also show SC at $T_c = 2.7$ and 3.8 K, respectively. Studies in the early stage have disclosed that the presence of a superstructure lowers T_c, which is related to the disorder effects due to the incommensurate ordering of two different types of conformations of terminal ethylene groups in ET molecules. Such disorder effects have been systematically investigated also by alloying different anions,[50] and a theoretical explanation was given.[51]

There are other similar polytypes classified as subfamilies of the β-type, i.e., β'- and β''-types, according to the degree of the anisotropy of transfer integrals, where the geometrical feature of the molecular arrangements are all the same. In sharp contrast to the above ordinary β-type materials, β'-ET_2X behave as semiconductors for $X = AuCl_2$[52] and IClBr and AF

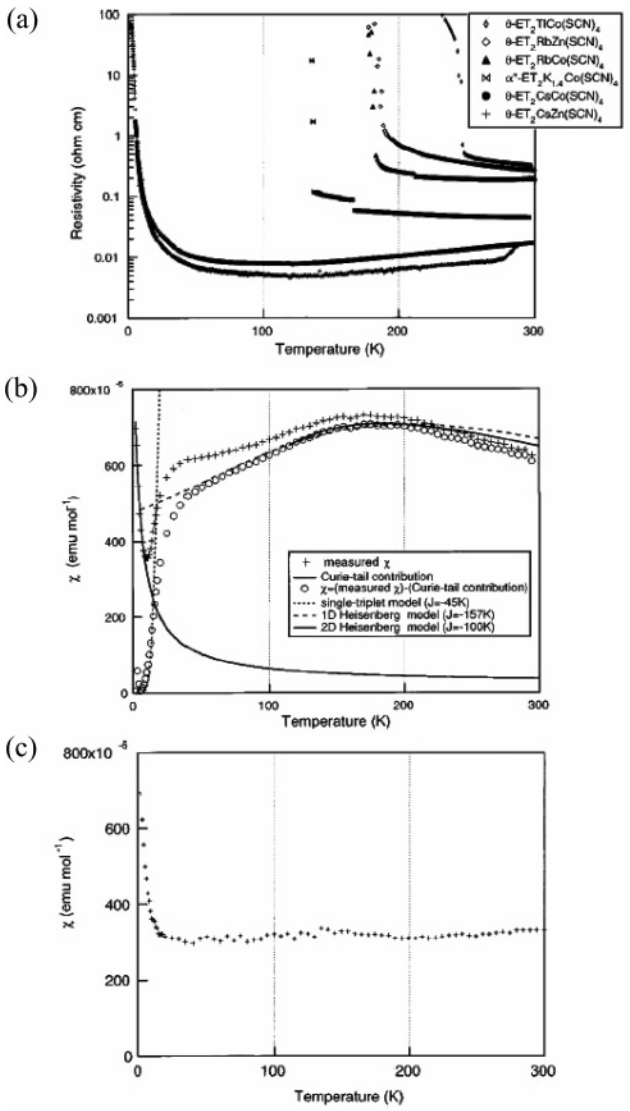

Figure 14. (a) Electrical resistivity, ρ, of several members of θ-ET_2X, (b) magnetic susceptibility, χ, of θ-$ET_2RbZn(SCN)_4$, and (c) χ, of θ-$ET_2CsZn(SCN)_4$. (Reprinted with permission from ref 47. Copyright 1998 The American Physical Society.)

insulators for $X = ICl_2$,[53] whereas β''-ET_2X ($X = AuBr_2$,[54] ICl_2,[55] and AuBrI[56]) are metallic but no sign of SC state is found up to now.

3.3.3. κ-Type

The family of κ-ET_2X has been studied in great detail because of its unique and interesting properties. They are very sensitive to the effective pressure as shown in their phase diagram Figure 15, extensively studied by Kanoda and collaborators.[57,58] It is seen that an AF insulating ground state has a first-order phase boundary with a SC ground state as a function of pressure. This AF state has a commensurate structure to the lattice; therefore, the insulating behavior in this system is considered to be due to the Mott insulator.[59] Recently, it has been disclosed that this sharp boundary between the insulating state and metallic state persists even above T_c and T_N with the critical end point[60] (see Figure 15). Above this point of temperature, the insulating state is transformed into the metallic state

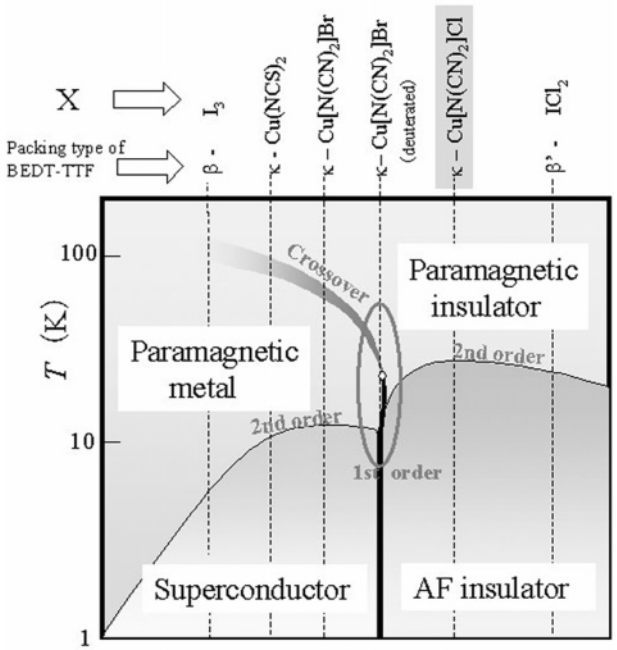

Figure 15. Kanoda's experimental phase diagram of κ-ET_2X[57,58] (courtesy of K. Kanoda).

gradually. The isostructural family based on BETS molecules, κ-$BETS_2X$, has a metallic character independent of anions as expected from a smaller U_{BETS} value. One can consider that they are located in the metallic region of Kanoda's phase diagram, and actually κ-$BETS_2GaBr_4$ has a SC phase with T_c as low as 1 K.[61]

κ-$BETS_2FeCl_{4-y}Br_y$ containing mangetic ions show properties different from the Ga-containing compounds.[46] In these systems, the AF ordering of Fe spins takes place at 4 K and 1 K for $X = FeBr_4$ and $FeCl_4$, respectively, whereas the π-electronic system remains metallic, and in the former SC sets at T_c = 1 K. As we will see in section 3.3.4, this is in sharp contrast to the effect of magnetic ions in their λ-type analogue where insulating phases are considerably stabilized by introducing the d spins. Very recently, SC under high magnetic field (H = 10−15 T) with the maximum T_c of 0.4 K is observed in κ-$BETS_2FeBr_4$,[62] only when H is applied exactly parallel to the BETS layer, which seems to be essentially the same phenomenon found first in λ-$BETS_2FeCl_4$ (see next).

3.3.4. λ-Type

λ-$BETS_2X$ system also shows a variety of ground states, which can be categorized depending on whether X contains magnetic Fe ion or not. First, the phase diagram by Tanaka et al. for $X = GaCl_{4-y}Br_y$ is shown in Figure 16a, where increase of the bromine content y corresponds to the expansion of the unit cell volume and then interpreted as an effective "inverse pressure" effect.[63] SC and insulating phases are next to each other at low temperatures as the effective pressure is varied, which is analogous to the phase diagram of κ-ET_2X in Figure 15. However, the magnetic behavior in the insulating phase is different to each other, where κ-ET_2X shows AF ordering at around 20 K[57,59] while λ-$BETS_2X$ show a maximum in χ at similar temperatures but without any signal of clear AF so far.

As for $X = FeCl_{4-y}Br_y$, on the other hand, a sharp first-order MI transition takes place for $X = FeCl_4$ together with an AF ordering between spins on the Fe ions, in striking contrast to $X = GaCl_4$ with SC ground state (see Figure 16a) although they have almost the same band parameters. Their phase

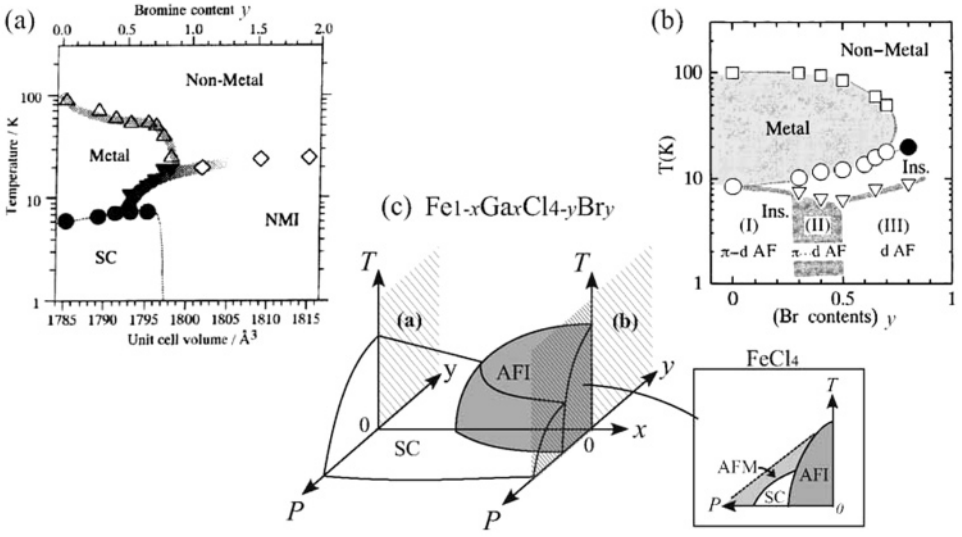

Figure 16. Experimental phase diagram of λ-$BETS_2X$ with (a) $X = GaCl_{4-y}Br_y$ (Reprinted with permission from ref 63. Copyright 1999 The American Chemical Society.); (b) $X = FeCl_{4-y}Br_y$ (Reprinted with permission from ref 64. Copyright 1998 The American Physical Society.); and (c) $X = Fe_xGa_{1-x}Cl_{4-y}Br_y$. The phase diagram on the plane of (external) pressure, P, and temperature, T, for $X = FeCl_4$ is shown together in the inset. Triangles in (a) and open squares in (b) correspond to the resistivity maxima and are not phase boundaries. In (a), the diamonds show the temperature where the magnetic susceptibility shows a maximum, where NMI stands for the postulated nonmagnetic insulating state. In (b), in the AF insulating phase, simultaneous AF and MI transition takes place in the region (I), while the two become separate in the larger y-region. The direction of the magnetic easy axis differs between the regions (II) and (III), which suggests the change in the degree of the π-d coupling. In (c), SC, AFI, and AFM stands for superconducting, antiferromagnetic insulating, and antiferromagnetic metallic phases, respectively.

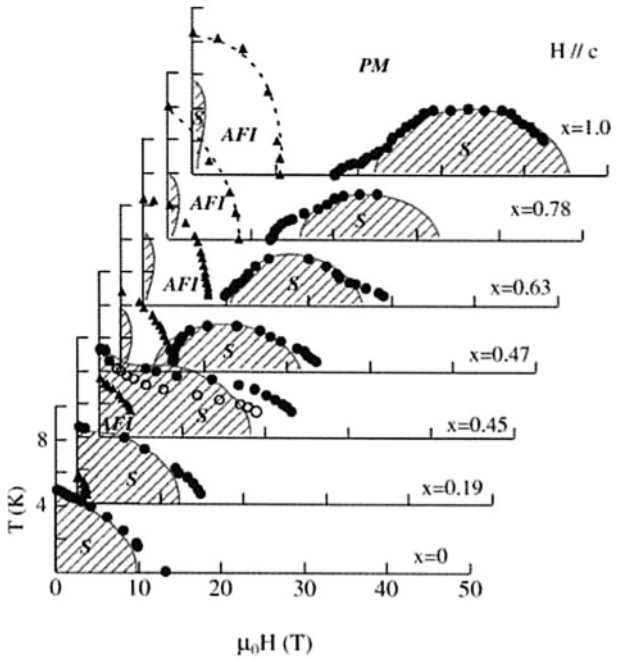

Figure 17. Experimental phase diagram of λ-$BETS_2X$ with $Fe_xGa_{1-x}Cl_4$ under high magnetic field. PM, AFI, and S denote the paramagnetic metallic, antiferromagnetic insulating, and superconducting phases, respectively. (Reprinted with permission from ref 69. Copyright 2003 The Physical Society of Japan.)

diagram is shown in Figure 16b,[64] where by increasing y the concomitant MI and AF transition at $y = 0$ branches into two different second-order transition lines. The region corresponding to the higher effective pressure than $y = 0$ is studied by actually applying external pressure to the $X = FeCl_4$ sample, whose phase diagram is shown in the inset of Figure 16. It turned out to be metallic even under the AF ordering of Fe spins below some temperature,[65] and at lower temperatures, the SC phase sets in coexisting with AF ordering of the anions.[66] This metallic region is similar to κ-$BETS_2FeY_4$ compounds mentioned above.

Furthermore, Tanaka et al.[67] succeeded in synthesizing a series of mixed crystals of the Ga- and the Fe-containing systems, with $X = Fe_xGa_{1-x}Cl_{4-y}Br_y$. The experimental phase diagram is shown in Figure 16c, where one can see that the electronic properties of two families, Ga- and the Fe-containing systems, are smoothly connected to each other.

The Fe-containing samples show a special SC state in the presence of strong external magnetic field, first found in $X = FeCl_4$ when $H = 18-41$ T is applied exactly parallel to the conducting plane, called the field-induced SC state.[68] The $H-T$ phase diagrams for $X = Fe_xGa_{1-x}Cl_4$ revealed by Uji et al. are shown in Figure 17,[69] for different values of x (the $H = 0$ properties are those along the x axis in Figure 16c), where one can see that the value of H necessary to attain the field-induced SC is a monotonic function of x and the SC phase at high H in $X = FeCl_4$ is linked to the zero field SC phase in $X = GaCl_4$.

3.3.5. α-Type

There exist two characteristic members in this family based on ET molecules, α-ET_2I_3 and α-ET_2M

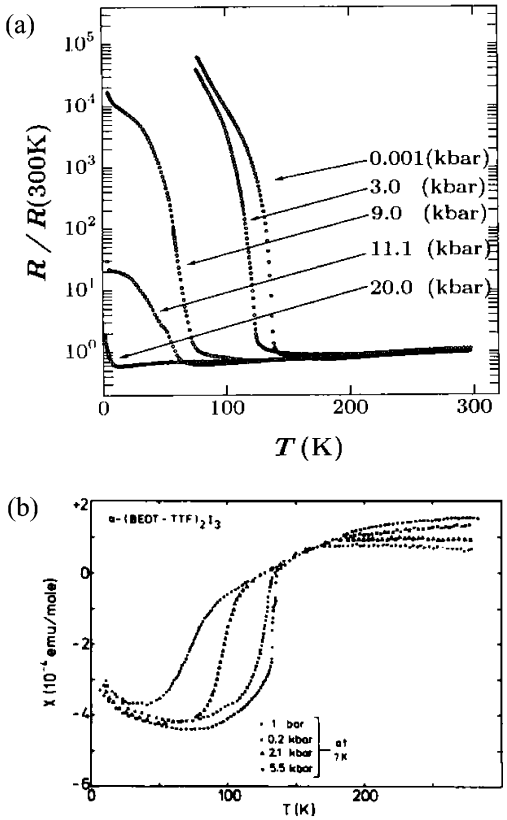

Figure 18. (b) Electrical resistivity, ρ (Reprinted with permission from ref 71. Copyright 2000 The Physical Society of Japan.), and (b) magnetic susceptibility, χ (Reprinted with permission from ref 72. Copyright 1986 The American Physical Society.) of α-ET_2I_3 under various values of hydrostatic pressure.

$Hg(SCN)_4$. In the case of α-ET_2I_3, the temperature dependence of ρ shows a sudden increase below around 130 K[70,71] accompanied by a sharp drop of χ,[72] as shown in Figure 18. Other α-ET_2X salts with $X = I_2Br$, IBr_2, $Cu(NCS)_2$, etc., and some of the α-$BETS_2X$ also show similar physical properties which can be categorized into the same group, where the BETS compounds have lower MI transition temperatures than the ET compounds.[43] On the other hand, in the case of mercury containing α-ET_2M $Hg(SCN)_4$ with M = K, Rb, Tl, and NH_4, metallic ground states are generally stabilized; depending on the ratio of lattice constants in the 2D ET plane, either a SC ground state or a density-wave-like anomalous state have been observed at low temperatures.[73] These two groups have been known from more than 15 years; however, the cause of the MI transition in α-ET_2I_3 has not been understood until recently (see section 5.2), and the anomalous state in α-ET_2M $Hg(SCN)_4$ is still not yet fully understood, despite numerous experimental as well as theoretical studies.

4. Electronic Structures and Classification of A_2B Compounds

To understand systematically the various electronic properties found in the previous section, considerations on the band structure of each compound and its classification are crucial. They will provide a clear starting point for the description of the electronic

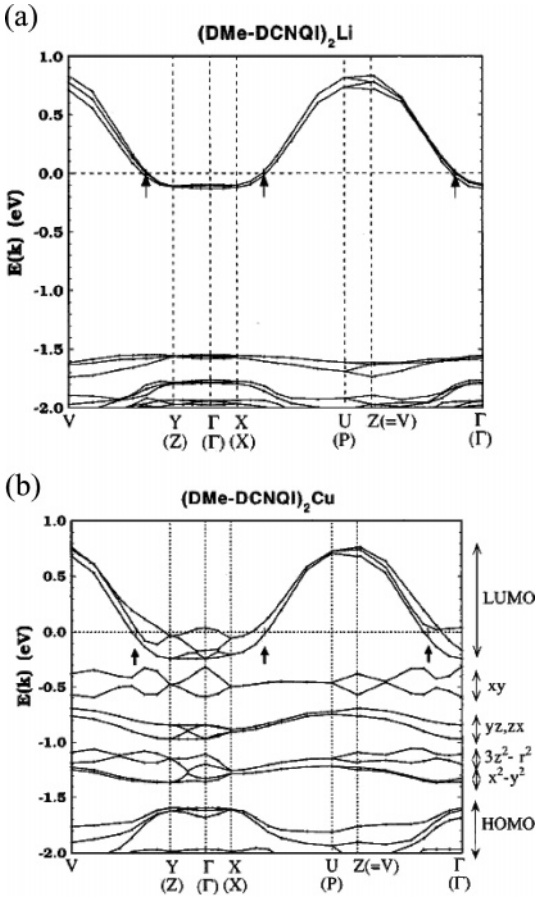

Figure 19. Results of LDA band structure calculations for (a) $(DMe\text{-}DCNQI)_2Li$ and (b) $(DMe\text{-}DCNQI)_2Cu$. (Reprinted with permission from ref 8. Copyright 1995 The American Physical Society.)

states before considering the electron correlation and other effects discussed in the subsequent sections.

4.1. $DCNQI_2X$

In this family, DCNQI molecules are arranged in 1D arrays, which are coupled three-dimensionally through X atoms. The LDA band structure in the case of $(DMe\text{-}DCNQI)_2Li$ is shown in Figure 19a, which is typical for the X = Ag, Li systems[8,9] The energy levels near the Fermi level for such X = Li, Ag compounds can be reproduced essentially by the tight-binding fitting with the values of the intrachain and interchain transfer integrals, $t = 0.15-0.25$ eV and $t_\perp = 0.01-0.03$ eV, respectively, which depend on the family members.[9] This band is constructed by the π orbital of DCNQI molecules and well separated in energy from the orbitals of Ag or Li, and then if we neglect the smaller $t_\perp$, the π band is a simple 1D quarter-filled band as was shown in Figure 2b.

In $DCNQI_2Cu$, by contrast, the π orbital and the d orbital are close to each other in energy and hybridize, which results in a complicated band structure as can be seen in Figure 19b,[8,9] where the LDA band structure of $(DMe\text{-}DCNQI)_2Cu$ is shown. There, electrons are transferred from the Cu d_{xy} orbital to the DCNQI π band, which results in the average valence of nearly $(DCNQI^{2/3-})_2Cu^{4/3+}$, so that a filling close to 1/3 in the π band and 5/6 in the d_{xy} orbital is realized. Here, d_{xy} orbital is well separated from other

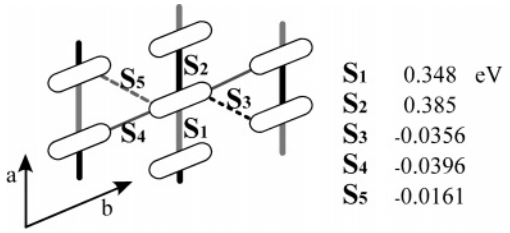

Figure 20. Spatial arrangement of TM molecules in TM_2X, where elongated circles represent TM molecules. The transfer integrals calculated by the extended Hückel scheme are shown for $TMTSF_2BF_4$.[74]

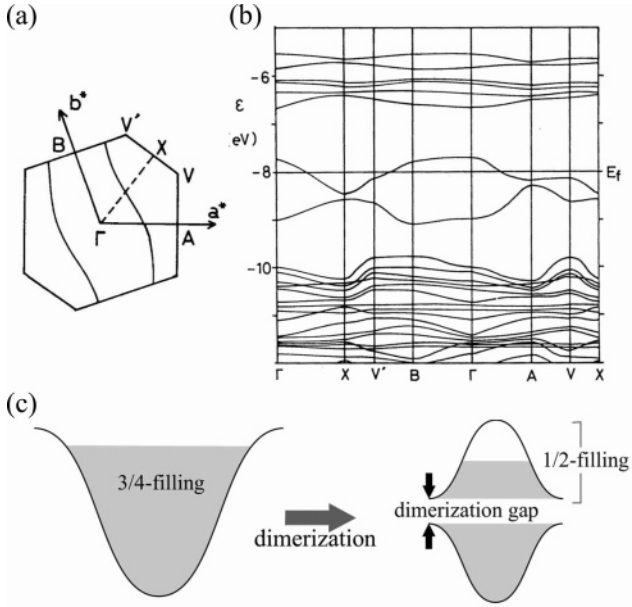

Figure 21. (a) Fermi surface and (b) tight binding band structure calculated by extended Hückel scheme for $TMTSF_2X$ (Reprinted with permission from ref 74. Copyright 1982 The Chemical Society of Japan.), and (c) schematic representation of the 1D band structures with and without dimerization (the case without dimerization is the same as Figure 2a).

d_{yz} and d_{zx} orbitals due to the crystal field effects from the tetrahedron of surrounding N atoms of DCNQI under Jahn–Teller distortion.[11] The degree of distortion affects the d_{xy} level, and presumably the amount of charge transfer, as well.

4.2. TM_2X

The spatial arrangement of the TM molecules in TM_2X is shown in Figure 20, where the values of transfer integrals estimated by the extended Hückel approximation are about 10 times larger in the stacking direction than in the interchain direction.[39,74] This results in an open Fermi surface as shown in Figure 21a with a good nesting condition. There are two TM molecules in the unit cell with a slightly dimerized structure, leading to a band structure with two HOMO bands near the Fermi energy, as shown in Figure 21b. The schematic representation of the band structure of a 1D dimerized chain but without interchain transfer is shown in Figure 21c. The larger the dimerization, the more the two bands split, and then a gradual crossover happens in an effective way from the 3/4-filling of the two bands as a whole toward the half-filling of the upper

Table 2. Transfer Integrals for θ-ET_2X Calculated by the Extended Hückel Scheme in Units of 10^{-2} eV[a]

X	TlZn	TlCo	Cu_2	$Cd_{0.66}$	RbZn	RbCo	CsZn	CsCo	I_3		$Au(CN)_4$
p	9.55	10.0	7.94	−7.7	9.4	9.9	10.8	10.6	11.7	4.2	2.43
c	−4.7	−4.8	−3.0	−3.5	−2.4	−3.3	−1.0	−0.49	2.2	6.4	6.28

[a] Those for $X = MM'(SCN)_4$ (M = Tl, Rb, Cs, M' = Zn, Co),[79,80] $Cd_{0.06}(SCN)_2$,[79] and $Cu_2(CN)[N(CN)_2]_2$,[81] are indicated as MM', $Cd_{0.06}$, and Cu_2, respectively. For θ-ET_2I_3, the values by two different groups are shown; Mori[82] (left) used the semiempirical parameters including the 3d orbitals of the sulfer atom, whereas Kobayashi[83] (right) excluded the 3d orbitals. Those for θ-$DIETS_2Au(CN)_4$[84] are also shown as $Au(CN)_4$.

Table 3. Transfer Integrals of β-ET_2X Calculated by the Extended Hückel Scheme in Units of 10^{-2} eV[85] [a]

X	I_3	I_2Br	$ICl_2(\beta')$	$AuCl_2(\beta')$	$AuBr_2(\beta'')$
p_1	−24.5	−23.9	−27.2	−26.4	9.6
p_2	−8.4	−8.9	1.6	2.0	8.7
q_1	−12.7	−12.5	−6.6	−10.0	1.5
q_2	−6.8	−6.7	−10.0	−6.5	6.5
c	5.0	5.2	−1.6	−2.3	15.0

[a] The sub-families, β' and β'', are indicated in the parenthesis.

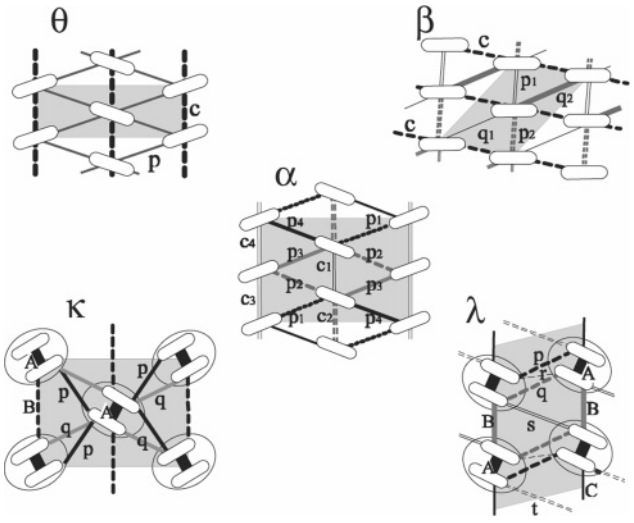

Figure 22. Schematic representation of the geometry of transfer integral between molecules in the unit cell for different polytypes of ET_2X and $BETS_2X$. The values of the transfer integrals are in Tables 2−6.

band. This is in contrast to the case of $DCNQI_2X$ with X = Ag and Li as seen in section 4.1, which has a single quarter-filled band free from dimerization.

4.3. Two-Dimensional Systems: ET_2X and $BETS_2X$

The anisotropy of transfer integrals for each polytype of this families is shown in Figure 22, where the corresponding values of transfer integrals estimated by the extended Hückel approximation are given in Tables 2−6. The θ-type structure with two molecules in a unit cell is the simplest; there are only two different transfer integrals, uniform along each direction. In the case of the β-type structure similarly with two molecules per unit cell, however, the transfer integrals are not uniform, i.e., an alternation exists in two directions with resultant five transfer integrals. (TM_2X discussed in section 4.2 belongs to this β-type structure as seen in Figure 20.) On the other hand, in κ- and λ-type structures with four molecules in a unit cell, it is seen that there exists a particular transfer integral with large absolute value.

Table 4. Transfer Integrals of κ-ET_2X Calulated by the Extended Hückel Scheme in Units of 10^{-2} eV, Given by Different Groups, (a),[86] (b),[87] and (c)[88] [a]

(a)

X	h_8-Cl	h_8-Br	$Cu(NCS)_2$
A	−27.3	−26.5	−27.2
B	−10.4	−9.8	−11.1
p	−10.5	−10.9	−11.9/10.5
q	3.9	3.8	1.8/−3.1

(b)

X	d_8-Cl	h_8-Cl	h_8-Br
A	−30.42	−30.06	−28.50
B	−11.45	−11.48	−10.62
p	−10.94	−11.07	−11.36
q	4.27	4.24	4.00

(c)

X	$Cu(NCS)_2$	I_3
A	−25.7	−10.92
B	−10.5	−2.46
p	−11.4/10.0	−5.05
q	1.7/2.9	1.85

(d)

X	$FeBr_4^K$	$FeCl_4^K$	$FeCl_4^M$
A	−23.90	−24.27	−11.83
B	−8.253	−9.735	−7.34
p	3.598	2.067	5.68
q	−0.282	−1.445	−2.66

[a] In (d), those of κ-$BETS_2X$ are shown where those calculated by Kobayashi[89] and Mori[82] are indicated by the superscripts "K" and "M", respectively.

Table 5. Transfer Integrals of λ-$BETS_2X$ Calculated by the Extended Hückel Scheme in Units of 10^{-2} eV[a]

X	$GaCl_4^K$	$FeCl_4^K$	$FeCl_4^M$
A	−27.38	−27.74	−13.39
s	−4.896	−5.07	−11.93
t	−0.654	−0.391	−1.93
C	−8.041	−8.29	−12.41
B	−11.14	−11.51	−10.58
p	2.058	1.79	1.93
q	4.011	3.785	5.28
r	−3.429	−3.69	−5.38

[a] Those by Kobayashi[89] and Mori[82] are indicated by the superscripts "K" and "M", respectively.

The pairs of molecules connected by this large transfer integral can be considered as dimers. Reflecting these differences, the band structure of each polytype has characteristic feature as shown in Figure 23, where the resultant Fermi surface is also shown together.

The first attempt to find out relationships between different polytypes was carried out by Kino and

Table 6. Transfer Integrals of α-ET_2X Calculated by the Extended Hückel Scheme in the Units of 10^{-2} eV[90,91]

X	$KHg(SCN)_4$	I_3
c_1	−1.9	−3.0
c_2	−6.8	−4.9
c_3	1.1	1.8
c_4	1.4	1.8
p_1	10.0	2.3
p_2	9.7	6.2
p_3	−13.3	14.2
p_4	−13.2	12.3

Fukuyama.[12,75] They proposed a generic model for ET_2X with four molecules in the unit cell which could approximately represent both κ- and α-type in Figure 22, by making some simplifications to emphasize the role of two particular important transfer integrals. In the κ-type structure the degree of dimerization represented by $|t_A|$ (see Table 4) is crucial to understand their electronic properties, and when $|t_A|$ is large the electronic structure is found to be well reproduced by regarding each dimer as a lattice site.[76] On this basis, an effectively half-filled "dimer model" on an anisotropic triangular lattice had been introduced,[76] on which the subsequent investigations are based[57,77] (see section 6.1). In the α-type structure, the transfer integral t_{p1} (see Table 6), which is the one that varies most among different members of this family, is regarded as a key parameter that controls the degree of overlap between upper two bands.

However, this simplified model of Kino and Fukuyama has limitations in that the oversimplification on the transfer integrals other than t_A and t_{p1} could not reconcile with the more generic parametrization to classify systematically the difference between many other different polytypes. Therefore, Hotta[78] proposed another model that could classify all the polytypes in Figure 22. In this model, any simplification or specification of the original transfer integrals is not made, except taking the limit of large dimerization for the κ- and λ-type structures, i.e., considering dimer models for these two polytypes. Then the polytpes can be devided into two groups; one is the θ- and β-type compounds with two molecules in the unit cell and the other is the strongly dimerized κ- and λ-type compounds with four. Then 3/4-filled models for the former and the half-filled dimer models for the latter again becomes the anisotropic triangular shape, as shown schematically in Figure 23. We see that the models for the θ- and κ-type structures have two kinds of transfer integrals (t, $t_1' = t_2' = t_3' = t_4' \equiv t'$), whereas for the β- and λ-type structures they have five different ones (t, $t_1' \sim t_4'$).

The α-type structure not included in Figure 23 has some complications within such picture; there are two different categories represented by α-ET_2I_3 and α-ET_2M $Hg(SCN)_4$, which we call α-I_3-type and α-*M* Hg-type, respectively. In the former, two transfer integrals, t_{p3} and t_{p4}, are significantly larger than the others, as seen in Table 6, whereas in the latter case, four transfer integrals $t_{p1} \sim t_{p4}$ all have similar magnitude, as shown schematically in Figure 24 together with their band structures and Fermi surfaces.

The features of the band structures all together will be summarized in the following.

1. In θ- and β-type structures, there are two bands in the Brillouin zone since there are two molecules in the unit cell, and the Fermi level is located in the higher band.

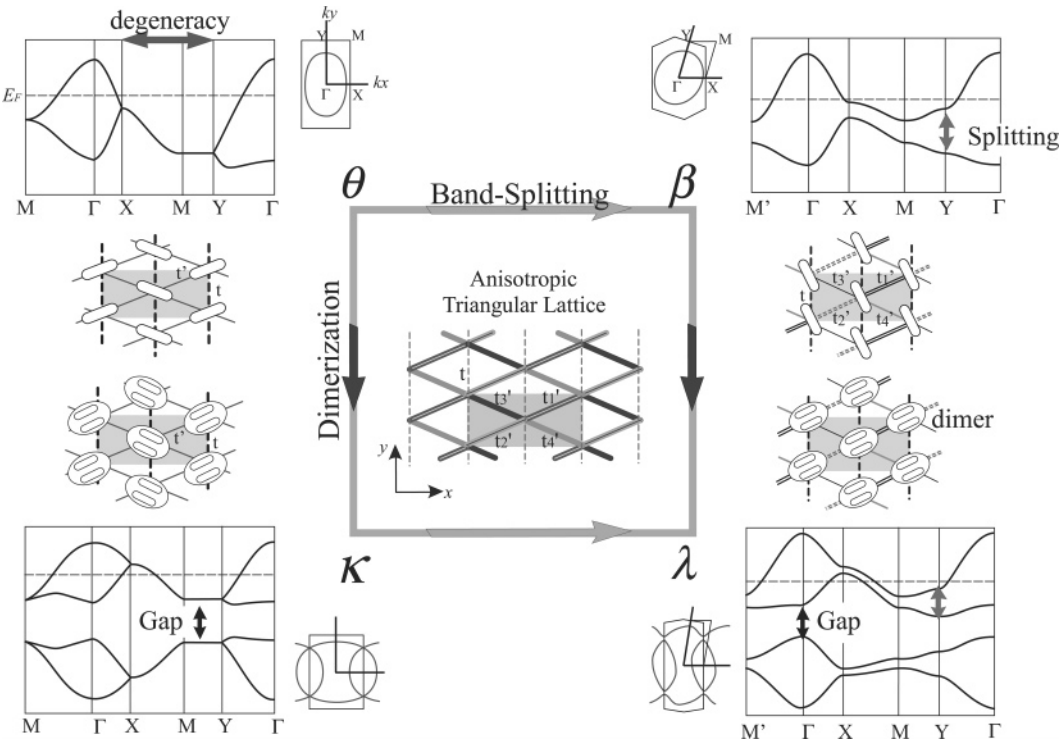

Figure 23. Relationship between different polytypes in 2D molecular solids based on the anisotropic triangular lattice shown in the center.

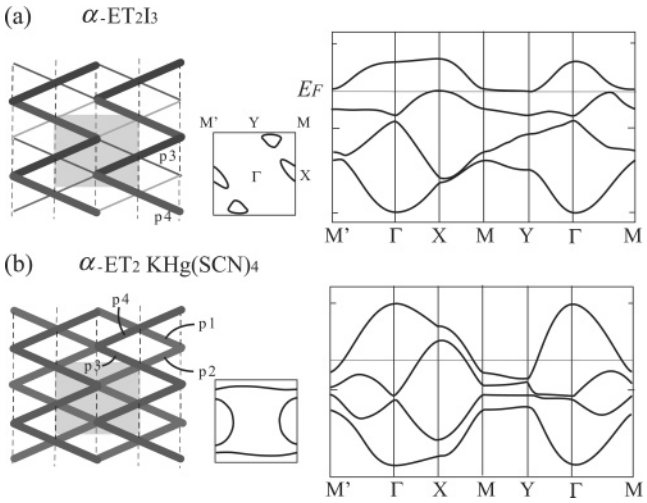

Figure 24. Simplified 2D plane of (a) α-ET_2M $Hg(SCN)_4$ and (b) α-ET_2I_3, together with their band structures and Fermi surfaces.

(a) In θ-type, there is a degeneracy of the two bands along the Brillouin zone boundary and then these two bands are not separated. Hence, the bands as a whole are considered to be 3/4-filled.

(b) In β-type, the degeneracy of the energy bands along the Brillouin zone boundary is lifted due to the nonuniform values of neighboring transfer integrals. If the band splitting at the zone boundary is not appreciable, these bands are effectively 3/4-filled. However, if this splitting is large compared to the bandwidth of each band, the higher band is solely regarded as effectively half-filled.

(c) The sub-families of β-type structures found in the actual solids, β-, β'-, and β''-types, have different degree of anisotropy among their five transfer integrals; in the β'-type structure, there is a significantly large transfer integral, t_{p1}, whereas in the β''-type structure, the transfer integral in one direction, t_c, has a large value. Such anisotropy is reflected in their band structures as shown in Figure 25, where they are classified according to the degree of band splitting. β''-type has the smallest degree of band splitting where both of two bands cross the Fermi level, but only the highest band does in β-type with modest band splitting, and in β'-type the band splitting becomes the largest. Therefore, a gradual crossover happens as $\theta \rightarrow \beta'' \rightarrow \beta \rightarrow \beta'$, from the 3/4-filled to half-filled in an effective way. This is in analogy with the 1D case explained in Sec. 4.2 for $DCNQI_2X$ (X = Ag, Li) and TM_2X families, where the dimerization along the chain direction results in the band splitting (see Figure 21c).

2. In κ- and λ-type structures, there are four bands in the Brillouin zone reflecting four molecules in the unit cell, which are grouped into two with clear energy separation. This grouping is due to the strong dimerization, in which case two groups can be treated independently as a first approximation. The upper two bands consisting of antibonding dimer orbitals have similar energy dependences in the Brillouin zone to those of the θ- and β-type structures, respectively. This indicates that dimers in κ- and λ-type structures play similar roles to those of molecules in θ- and β-type structures, respectively.

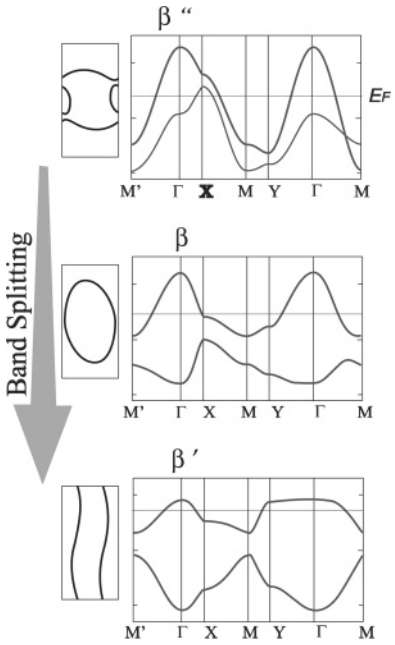

Figure 25. Band structures and Fermi surfaces of three sub-families in β-type.

(a) In the case of κ-type, the effective transfer integral between dimers is uniform along each direction and the partially degenerate bands of antibonding orbitals is considered to be half-filled as a whole.

(b) In the case of λ-type, depending on the degree of the lifting of the degeneracy of upper two bands along the zone boundary, the system is gradually transformed from half-filling to complete filling (band insulators) in the presence of the large splitting.

3. It turns out that there are variations in the α-type structure.

(a) In the case of α-I_3 type, only if the two large transfer integrals, t_{p3} and t_{p4}, are taken into account, a zigzag chain structure is formed. The four bands are essentially separated with completely filled three bands and an empty single band, and then a band insulating state is expected. In reality, a semimetallic state with small pockets is realized due to the small modifications of the band structure coming from other transfer integrals.

(b) In the case of α-MHg-type, four transfer integrals, $t_{p1} \sim t_{p4}$, have similar absolute magnitudes. The larger values of t_{p1} and t_{p2} compared to α-I_3 type lead to appreciable overlap between the upper two bands. The difference between the two α-type structures regarding the degree of band splitting is just the same as the case of κ- and λ-type ones. What differs is that the dimer structure is absent in the α-type structures, then the separation between upper two and lower two bands are not large.

All these features of band structures depending on polytypes can be expressed as those of density of states as schematically shown in Figure 26; the polytypes are categorized into three groups as, two-band systems (θ, β), four-band systems without dimerization gap (α), and four-band systems with dimerization gap (κ, λ). Within each group, the polytypes are classified according to the degree of band splitting which characterizes the nature of their one-particle state. This can be formulated more

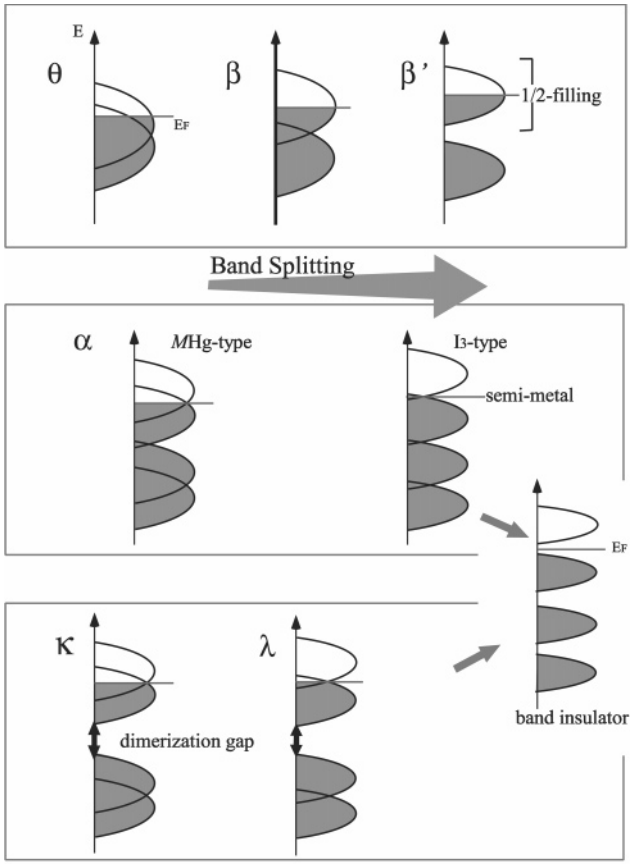

Figure 26. Relationship between different polytypes in 2D molecular solids. Density of states are shown schematically to understand intuitively the meaning of band splitting. Polytypes are classified into three groups; those with only two bands, with four bands but without dimerization, both with four bands and with dimerization, from top to bottom, respectively. In the limit of large band splitting, the latter two systems are expected to become a band insulator.

Table 7. Relationships between Transfer Integrals of the Original Polytypes and Those of the Anisotropic Triangular Lattice in Figure 23, t, t'~t'_4

	θ	β	κ	λ	α
t	t_c	t_c	$t_B/2$	$2(t_p + t_q - t_r)$	$t_{p1}/2$, $t_{p2}/2$
t'_1	t_p	t_{p1}	$(t_p - t_q)/2$	t_s	$(t_{p1} - t_{c1})/2$
t'_2	t_p	t_{p2}	$(t_p - t_q)/2$	t_t	$(t_{p3} - t_{c3})/2$
t'_3	t_p	t_{p3}	$(t_p - t_q)/2$	t_C	$(t_{p2} - t_{c2})/2$
t'_4	t_p	t_{p4}	$(t_p - t_q)/2$	t_B	$(t_{p4} - t_{c4})/2$

explicitly by the transfer integrals in the anisotropic triangular lattice model in Figure 23.[78] The transfer integrals of each polytype in Figure 22 are mapped to those of the anisotropic triangular lattice (t, $t'_1 \sim t'_4$) as in Table 7.

In the following sections, starting from the noninteracting band structures explained in this section, theoretical understandings of the physical properties of A_2B systems mainly at low temperarures are given by introducing the electron correlation and other effects. More detailed experimental information (mostly recent one) than in section 3 is also provided for some specific topics.

5. Charge Ordered States

The CO state, which is one of the limiting cases realized in quarter-filled system as mentioned in section 2.2, is recently found to be ubiquitous in A_2B systems. The first clear experimental observation of CO in quarter-filled molecular crystals was given in the NMR measurement on (DI-DCNQI)$_2$Ag performed by Hiraki and Kanoda.[92] On the other hand, independently, Seo and Fukuyama[15] predicted the existence of CD among molecules in another system TMTTF$_2X$, which are the members of the well-studied family of the Bechgaard salts. Afterward, the CO phenomenon has been extensively investigated hand in hand both experimentally and theoretically, and it turned out that CO frequently exists not only in such quasi-1D compounds but also in quasi-2D compounds as well.

In these cases, the crucial roles of Coulomb interaction, especially the long-ranged interaction, have been recognized through different theoretical studies on the extended Hubbard model in eq 1. In this section, we first review each system where CO was found and introduce main theoretical studies reported so far to understand them. We also point out some new problems associated with CO.

5.1. One-Dimensional Systems

We first explain CO states in 1D systems where experiments were first performed and comprehensive theoretical studies have been carried out motivated by the experiments.

5.1.1. Charge Order in DCNQI$_2X$ and TMTTF$_2X$

In DCNQI$_2X$ (X = Li, Ag) and TMTTF$_2X$, interchain transfer integrals are about 10 times smaller than the intrachain ones as we have seen in sections 4.1 and 4.2. Then the 1D version of eq 1 can be applied as the effective model as a first approximation

$$H = \sum_i \sum_\sigma (t(1 + (-1)^i \Delta_d) c^\dagger_{i,\sigma} c_{i+1,\sigma} + h.c.) + \sum_i U n_{i\uparrow} n_{i\downarrow} + \sum_i V n_i n_{i+1} \quad (2)$$

where the band filling is a quarter in terms of electrons and holes, for DCNQI and TMTTF compounds, respectively, which are equivalent in the case of eq 2. Here Δ_d is the degree of dimerization, which is absent in DCNQI$_2X$,[9] whereas Δ_d =0.1−0.05 in TMTTF$_2X$ according to the extended Hückel calculations.[39]

The case $\Delta_d = 0$ in eq 2, i.e., the 1D extended Hubbard model, has been studied from early days. Its ground state phase diagram obtained first by Mila and Zotos[93] using the numerical Lanczos exact diagonalization method is shown in Figure 27, where the metallic Tomonaga-Luttinger (TL) liquid phase and an insulating phase compete with each other. The insulating state is stabilized in the large U/t and V/t region, which is due to the Wigner crystal-type CO state.

It is noteworthy that the mean-field (MF) approximation to eq 2

$$n_{i\sigma} n_{i\sigma'} \rightarrow \langle n_{i\sigma} \rangle n_{i\sigma'} + n_{i\sigma} \langle n_{i\sigma'} \rangle - \langle n_{i\sigma} \rangle \langle n_{i\sigma'} \rangle \quad (3)$$

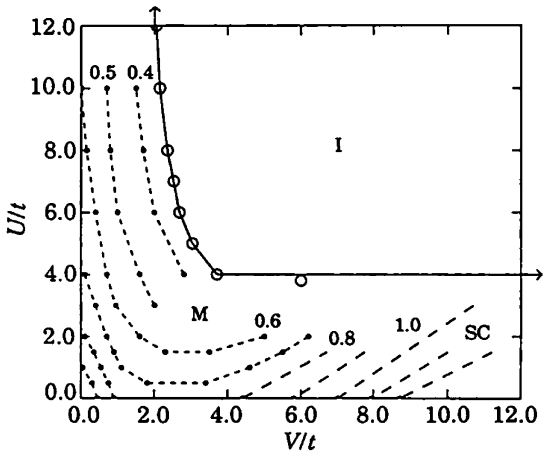

Figure 27. Ground-state phase diagram on the plane of U/t and V/t of the 1D extended Hubbard model. I, M, and SC denote the insulating (charge-ordered), metallic, and superconducting states, respectively. (Reprinted with permission from ref 93. Copyright 1993 EDP Sciences.)

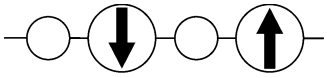

Figure 28. Schematic representation of the mean-field ground state of 1D extended Hubbard model with $\Delta_d = 0$ in the charge ordered state. The size of the circle and the arrows represent the charge density on each site and the spin moment, respectively.

provides a physical view of the ordered ground state in the compounds. The results show that when V exceeds a critical value, V_c, CD among sites with alternating "charge-rich" and "charge-poor" sites appears whose amount increases as a function of V, in accordance with the numerical study above. Besides, AF ordering between spin moments on the charge-rich sites appear as shown in Figure 28.[15] We must be careful that the quantum fluctuations are completely ignored in the MF calculations; the AF ordering seen above is actually destabilized but remains as fluctuations in numerical studies.[93,94] Nevertheless, in the actual compounds with appreciable interchain transfer integrals, AF long range ordering shows up at low temperatures as we will see later, in accordance with MF calculations for the ground state.

Equation 2 with $\Delta_d \neq 0$ was first examined to investigate the AF phase of $TMTTF_2X$ within the MF approximation.[15] (Studies with $\Delta_d \neq 0$ existed before but only for $V = 0$.[95]) The results show that, by increasing the value of V at a fixed value of U, an AF state between dimers (spin pattern along the chain direction is [↑ ↑ ↓ ↓]) with uniform charge density, interpreted as the DM insulating state, turns into a state both with CD and with spatial modulation of spin density as shown schematically in Figure 29. This state is also a kind of a CO state, but may be viewed as a coexistent state of the CO state and the DM state because of finite Δ_d.

Theoretical works to understand the effects of quantum fluctuations in eq 2 with $\Delta_d \neq 0$ have recently been carried out numerically as well as analytically. The phase diagram obtained by numerical calculations on the plane of U and V for a fixed

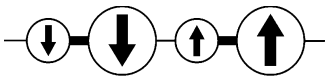

Figure 29. Schematic representation of the mean-field ground state of 1D extended Hubbard model with $\Delta_d \neq 0$ in the charge ordered state. The size of the circle and the arrows represent the charge density on each site and the spin moment, respectively.

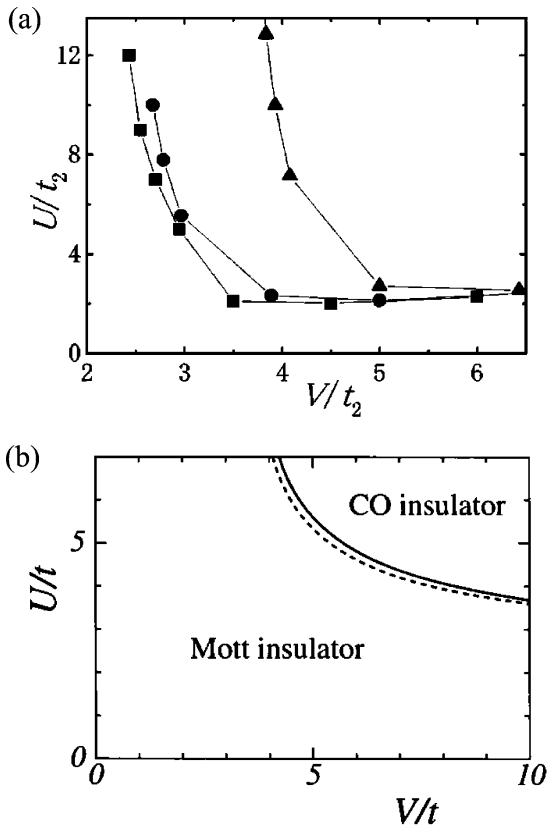

Figure 30. Ground-state phase diagrams of the 1D extended Hubbard model with $\Delta_d \neq 0$. In (a), the CO phase boundary for $\Delta_d = 0$ (squares), 0.052 (circles), and 0.194 (triangles) for a 16 sites system in a cluster mean-field calculation is shown, where $t_2 = t(1 + \Delta_d)$. (Reprinted with permission from ref 96, Copyright 2001 The American Physical Society.) In (b), the phase boundary for $\Delta_d = 0$ (dotted line) and 0.001 (solid line) calculated by the renormalization group method to eq 4 is shown. (Reprinted with permission from ref 98, Copyright 2001 The Physical Society of Japan.)

value of Δ_d is shown in Figure 30a,[96] where the metallic phase at $\Delta_d = 0$ (see Figure 27) is now replaced by the DM insulating phase, although a phase with Wigner crystal-type CD is still present in the large U and V region, which is the coexistence phase of CO and DM consistent with the MF study above. The AF ordering in MF calculations is destabilized in these calculations due to the quantum fluctuations, as in the $\Delta_d = 0$ case.

Studies based on the bosonization scheme have been carried out by Yoshioka et al.,[97,98] which is suitable for understanding 1D systems analytically where quantum fluctuations play important roles.[99] They made direct correspondence between eq 2 and the effective Hamiltonian expressed by phase variables, i.e., the phase Hamiltonian, represented as

$$\mathcal{H} = \mathcal{H}_\rho + \mathcal{H}_{\text{Umklapp}} + \mathcal{H}_\sigma \tag{4}$$

$$\mathcal{H}_\rho = \frac{v_\rho}{4\pi}\int dx\left\{\frac{1}{K_\rho}(\partial_x\theta_+)^2 + K_\rho(\partial_x\theta_-)^2\right\} \tag{5}$$

$$\mathcal{H}_{\text{Umklapp}} = -g_{1/2}\,\Delta_d\int \mathrm{d}x\,\sin 2\theta_+ + g_{1/4}\int \mathrm{d}x\,\cos 4\theta_+ \tag{6}$$

$$\mathcal{H}_\sigma = \frac{v_\sigma}{4\pi}\int dx\left\{\frac{1}{K_\sigma}(\partial_x\phi_+)^2 + K_\sigma(\partial_x\phi_-)^2\right\} \tag{7}$$

Here, θ_+ and ϕ_+ are the phase variables associated with the local density fluctuations of charge and spin with long wavelength, respectively, and $\Pi_\theta = -\partial_x\theta_-/2\pi$ and $\Pi_\phi = -\partial_x\phi_-/2\pi$ are the corresponding 'canonical momenta' which satisfy $[\theta_+(x),\Pi_\theta(x')] = i\delta(x-x')$ and $[\phi_+(x),\Pi_\phi(x')] = i\delta(x-x')$. $\mathcal{H}_\rho$ and $\mathcal{H}_\sigma$ describe the "charge part" and the "spin part" of the TL liquid, which is a characteristic metallic state in the interacting 1D systems, where (v_ρ, K_ρ) and (v_σ, K_σ) are the so-called TL parameters for each part, respectively. The coupling constants for the half-filled as well as the quarter-filled Umklapp scattering terms are calculated perturbatively from the weak-coupling regime as[97,98]

$$g_{1/2} \propto U - \frac{1-{\Delta_d}^2}{1+{\Delta_d}^2}\frac{a^2}{2\pi v_{\mathrm{F}}}\times \int \mathrm{d}\varphi\left(\sum_{\epsilon=\pm1}\left[2+2\sqrt{1+\epsilon\frac{1-{\Delta_d}^2}{1+{\Delta_d}^2}\cos\varphi}\right]\right)\frac{U(U-2V)}{t} \tag{8}$$

$$g_{1/4} \propto U^2(U-4V)/t^2 \tag{9}$$

where a and v_{F} are the lattice constant and the Fermi momentum, respectively. Through the renormalization group treatment on eq 4, the high energy part of this Hamiltonian is integrated out to describe low energy excitations whose nature is determined by the terms giving the largest renormalized coupling constants. The $g_{1/2}$ term is finite only when $\Delta_d \neq 0$ and produces the DM insulating state as has been pointed out by Emery.[100] On the other hand, the $g_{1/4}$ term induces the Wigner crystal-type CO state, as has been discussed earlier by different authors who introduced it phenomenologically.[101] These two terms, $g_{1/2}$ and $g_{1/4}$, compete with each other to open a charge gap. The phase diagram by this procedure is shown in Figure 30, which is consistent with the phase diagrams obtained by numerical calculations shown in Figures 27 and 30a.

Let us now turn to the experimental studies on the CO state in these 1D compounds, which was first detected in the ^{13}C-NMR line shape in $(DI\text{-}DCNQI)_2Ag$,[92] as shown in Figure 31. The resonance line at high temperatures splits into two at around 200 K upon cooling, where the electrical resistivity, ρ, changes its slope as seen in Figure 5 and in the derivative of the Arrhenius plot, i.e., in $\mathrm{d}(\ln\rho)/\mathrm{d}(1/T)$ curve.[102] This was assigned to the

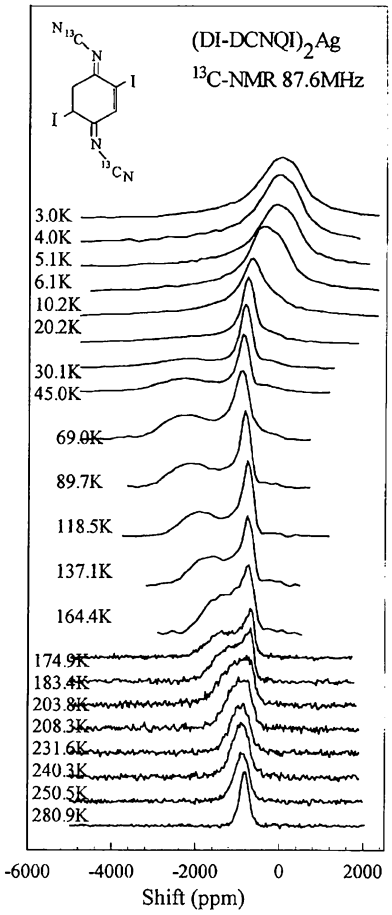

Figure 31. Observation of charge ordering in $(DI\text{-}DCNQI)_2Ag$ by means of ^{13}C-NMR. The resonance line is shown for different temperatures, where the charge disproportionation is seen to set in around 200 K. (Reprinted with permission from ref 92. Copyright 1998, The American Physical Society.)

emergence of two kinds of molecular sites with different charge densities, i.e., CD among the molecules which were all uniform at high temperatures, whose charge pattern is the Wigner crystal-type one as confirmed by X-ray diffraction measurements.[103] At a lower temperature of about 5 K, AF order sets in, which is the one among the localized spins on the "charge rich" sites.[30,92]

On the other hand, the localized state of the TMTTF compounds in the low-temperature region was believed to be due to the DM insulating state for a long time.[38,100] However, on the basis of ^{1}H-NMR measurements, Nakamura et al.[104] proposed a spin pattern [↑ 0 ↓ 0] along the chain direction, which is different from that expected from the DM state, [↑ ↑ ↓ ↓]. This lead to the theoretical proposal that CD exists in this compound, where the spin pattern becomes consistent with the ^{1}H-NMR analysis if the degree of CD is large enough (see Figure 29).[15] The existence of CO is now widely confirmed in TMTTF compounds; its first clear observation was by ^{13}C-NMR[105] where the resonance line splits into two as in $(DI\text{-}DCNQI)_2Ag$, and also by low-frequency dielectric measurements.[106] As a matter of fact, a trace of the transition had already been found earlier and was called "structureless transition" as noted in section 3.2, including the dielectric measurement at

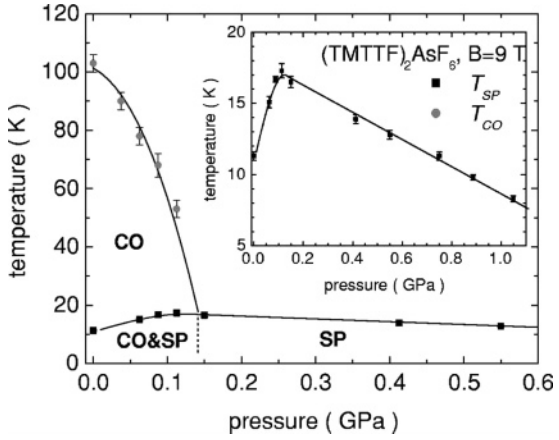

Figure 32. Pressure−temperature phase diagram of $TMTTF_2AsF_6$. CO and SP denote the charge ordered and spin-Peierls states, respectively, whereas CO&SP is the coexistent state of these two. (Reprinted with permission from ref 107. Copyright 2002 The American Physical Society.)

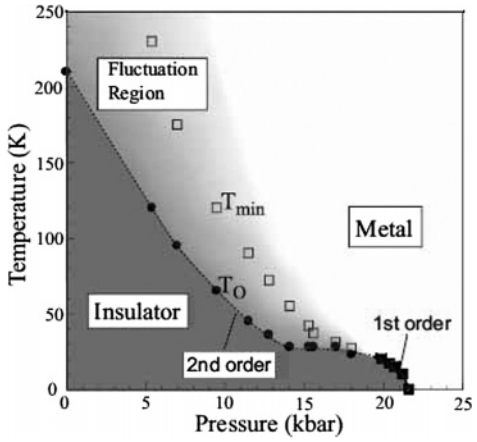

Figure 33. Pressure−temperature phase diagram of $(DI\text{-}DCNQI)_2Ag$[102] (courtesy of T. Itoh and K. Kanoda).

6.5 GHz,[41] although its origin was unknown at that time. It is noteworthy that recently the dielectric constant at very low frequency down to 100 Hz is found to show a Curie−Weiss behavior and to diverge at a temperature similar to the temperature where the NMR line starts to split,[106] which indicates that ferroelectricity is generated by the CO. This is considered to be due to the coexistent state of dimerization and CO shown in Figure 29, which possesses a macroscopic polarization if the pattern of the CD is in-phase for all TMTTF chains in the crystal.

The CO state in TMTTF compounds is quite fragile against external pressure. In $TMTTF_2AsF_6$, with the CO transition temperature of 100 K and where the SP state exists below 10 K,[105] the CO state is destabilized within 0.15 GPa and is transformed into the DM state while the SP state remains stable,[107] as shown in Figure 32. On the other hand, $TMTTF_2SbF_6$ shows a higher CO transition temperature of 150 K at ambient pressure with AF ground state coexisting with the CO, where the CO state is again destroyed under pressure of about 0.6 GPa.[108] There, magnetic properties at the ground state behave as AF → SP upon increase of pressure and extended version of the phase diagram in Figure 10 is suggested,[108] showing a re-entrant behavior for the ground state properties of the TMTTF salts as AF → SP → AF. This is unexpected when one considers the effect of pressure to increase the interchain transfer integral (and consequently the interchain exchange interaction), as has been discussed in Figure 10, since this should result in the stabilization of the AF state over the SP state,[109] opposite to what is seen in $TMTTF_2SbF_6$ at low pressure. Such complex behavior suggests that the electronic properties of the $TMTTF_2X$ compounds, and certainly the family of TM salts altogether, needs further investigations and reconsiderations; it is crucial to understand the role of the CO states on their properties in more detail by pursuing systematic investigations of the roles of long-range Coulomb interactions, interchain transfer integrals, and couplings to the lattice degrees of freedom discussed in the next subsection.

By applying pressure further, the interchain transfer integrals increase and become important in the TMTSF side of Jérome's phase diagram, where a dimensional crossover occurs.[110] There, a metallic state is realized, which is unstable toward the SDW state due to the nesting of the Fermi surface below around 10 K where the on-site Coulomb interaction U plays a main role. In such a weakly interacting regime, MF treatment of the 2D (quasi-1D) Hubbard model including the interchain transfer integrals successfully describes their properties even at finite temperatures, including the field-induced SDW phenomenon widely observed in $TMTSF_2X$.[2]

Recently, an experiment measuring the pressure effect on $(DI\text{-}DCNQI)_2Ag$ has disclosed that the CO state is suppressed also in DCNQI family but not so sensitively as in the TMTTF series, as seen in Figure 33.[102] An unexpected finding is the change of the order of phase transition, from a second order at low pressure to a first order at high pressure. Moreover, it is found that the resisitivity, ρ, in the metallic state realized near the complete suppression of CO obeys T^3-law indicating the onset of new type of liquid state whose cause is not understood at present. The pressure is naively expected to increase the value of the interchain transfer integrals as in the case of TM_2X; however, the origin of the different properties observed in these two families is still to be examined.

5.1.2. Electron–Phonon Interaction

Up to now, we have considered only the effects of electron−electron Coulomb interaction and neglected the electron−phonon interaction. However, it is known that the electron−phonon interaction plays important roles as well, particularly in 1D compounds, and as a matter of fact, it affects the electronic properties of $DCNQI_2X$ and $TMTTF_2X$ we have seen in section 5.1.1. One important effect of the electron−phonon interaction is to introduce the spontaneous dimerization in the originally nondimerized system leading to the DM state, as has been observed in many compounds including several $DCNQI_2X$ (see refs 1 and 30). In $DCNQI_2X$ (X = Li, Ag), the origin of the insulating behavior is either

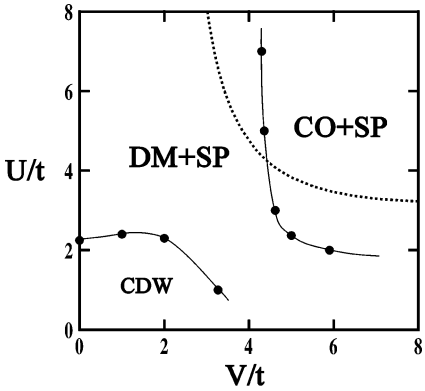

Figure 34. Ground-state phase diagram of eq 10 with $K = 1$ determined by density matrix renormalization group calculations.[111] CO+SP, DM+SP, and CDW denote the coexistence of CO and SP states, that of DM and SP states, and weak-coupling CDW states, respectively.

the CO state as explained in the previous subsection, or, such spontaneous DM state, where the lattice dimerization occurs concomitantly with the crossover to the insulating state. Another example of the effect which the electron−phonon interaction brings about is the SP state, also frequently observed in quarter-filled molecular solids. When a nonmagnetic state that emerges upon cooling below the MI phase transition temperature is accompanied by the lattice distortion of a period of four molecules (tetramization) in the chain direction, it is usually interpreted as a SP state.

To study theoretically the effects of the electron−phonon interaction in the quarter-filled 1D system, let us consider a model including the so-called Peierls-type or Su−Schrieffer−Heeger-type electron−phonon interaction, which modulates the transfer integrals in eq 2 as

$$\mathscr{H}_{\mathrm{P-H}} = \sum_{i,\sigma} t(1+u_i)(c_{i\sigma}^{\dagger}c_{i+1\sigma} + h.c.) + \frac{K}{2}\sum_i u_i^{\,2} + U\sum_i n_{i\uparrow}n_{i\downarrow} + V\sum_i n_i n_{i+1} \quad (10)$$

This will be called the extended Peierls−Hubbard model. Here u_i and K are the renormalized lattice distortion between sites i and $i+1$ and the elastic constant, respectively. When the electron−electron Coulomb interactions are weak, the conventional CDW state (with a period of four molecules) due to the Peierls instability is realized.[99] In the strongly correlated regime, however, two different kinds of SP states compete with each other. In Figure 34, the phase diagram for $K = 1$ determined by Kuwabara et al.[111] using the numerical density matrix renormalization group method is shown on the plane of U/t and V/t. The lattice distortions u_i's are treated as classical values and determined self-consistently. It is seen that there exist two kinds of coexistent state in the strongly correlated regime as shown schematically in Figure 35; the coexistent state of DM and SP which has already been known,[112] and the one with CO and SP which is newly found to be stabilized. The former is relevant to SP compounds such as MEM-$TCNQ_2$ and TEA-$TCNQ_2$ (see refs 1 and 112) and also to some of the DCNQI$_2X$ compounds noted above, whereas the latter is relevant to TMTTF compounds showing the SP transition at ambient pressure.[105,107]

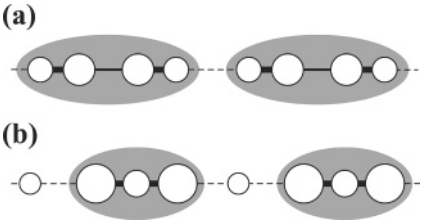

Figure 35. Schematic representation of coexistent state of (a) DM and SP, and (b) CO and SP. The size of circles and the thickness of bonds represent the charge density on sites and the lattice distortions, respectively. The spin singlet formation is schematically drawn by gray elipses.

These SP states should be affected by the two(or three)-dimensionality present in the actual compounds. It is known that interchain exchange interaction would destabilize the SP state and bring about the AF state.[109] In fact, the experiments show that pressure plays such a role, e.g., in Jérome's phase diagram for TM_2X (Figure 10). However, systematic understanding of the ground state properties between various compounds has not yet been achieved either theoretically or experimentally; the determining factor of which SP state is actually realized, and/or the interplay between the CO and DM states in the charge degree of freedom and the SP and AF states in the spin degree of freedom, is not fully understood.

Finally, we comment that there is another type of electron−phonon interaction, i.e., the Holstein-type one, which modulates the on-site potential energy, ϵ_i, with the cost of elastic energy

$$\mathscr{H}_{\mathrm{Holstein}} = \sum_i \left(\epsilon_i n_i + \frac{K}{2}\epsilon_i^{\,2}\right) \quad (11)$$

This interaction is due to the electron-molecular vibration (so-called e-mv) coupling mode[113] or due to the coupling to the anion.[114] It stabilizes the Wigner crystal-type CO state and then may be considered to enhance V effectively, although its energy scale is smaller compared to not only the electron−electron Coulomb interactions but also to the Peierls-type electron−phonon interaction.

5.1.3. DCNQI$_2$Cu

The DCNQI$_2X$ system with X = Cu is quite different from those with X = Li, Ag as we have seen in sections 3.1 and 4.1. Such unique features seen in the phase diagram in Figure 6 are due to the $\pi-d$ hybridization bringing about a certain degree of three-dimensionality, as disclosed first by Kobayashi et al.[11] In the metallic phase, the valence of Cu is close to +3/4,[115] and the apparently temperature independent behavior of the magnetic susceptibility χ seen in Figure 7 is recently found to consist of two temperature-dependent components of π and d orbitals with AF and ferromagnetic fluctuations, respectively.[116]

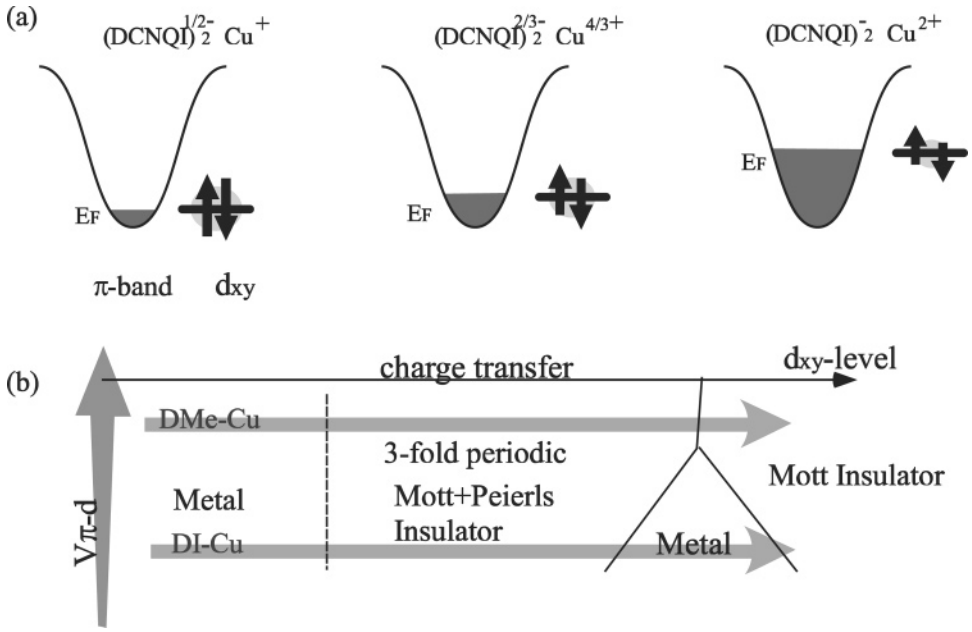

Figure 36. Schematic representation of the pressure effect in $DCNQI_2Cu$ interpreted as due to the upward shift of the d_{xy} level. (a) change in the relative energy of the π band and the d_{xy} level and (b) the resulting phase diagram as functions of energy of the d_{xy} level and the interchain Coulomb interaction between π and d electrons, $V_{\pi-d}$, are given.

On the other hand, in the insulating phase, the 3-fold periodic CD in the Cu chain appears as (Cu^+ Cu^+ Cu^{2+}),[35] which is compatible with the Peierls transition in the 1/3-filled single π band.[32] Vice versa, the Peierls transition of the π band introduces a periodic potential which makes the *d* band half-filled leading to its Mott insulating state, and then this charge localization is interpreted as a result of the cooperative transition of these two mechanisms.[117] Based on such a picture, the first-order nature and the reentrant behavior of the MI transition seen in Figure 6 is explained phenomenologically.[118,119] Another theoretical study by the slave-boson approach on the extended periodic Anderson model showed that such reentrant first-order MI transition is found to be realized in a certain range of the electron−phonon coupling constant.[120] We note that the 3-fold CO state seen in the Cu sites is very different from the CO state due to the intersite Coulomb interaction as in the X = Li, Ag systems. Theoretical calculations indicate that the 3-fold insulating state is hardly stabilized by the intersite Coulomb repulsions.[121]

An important effect of the external pressure is to distort the tetrahedron of surrounding N atoms of DCNQI further and then to shift the Cu d_{xy}-level upward by the crystal field effect, resulting in the increase in the amount of charge transfer from the *d*-level to the π-band, as shown schematically in Figure 36a. There actually is an experimental indication[32] as well as LDA first principle band calculation[122] suggesting the increase of the amount of charge transfer from Cu to DCNQI under pressure.

In iodine-containing compounds such as $(DI\text{-}DCNQI)_2Cu$ and $(BrI\text{-}DCNQI)_2Cu$, the sequences of MI transition have been observed when stronger pressure is applied as shown in Figure 8.[36] In this case, with the further increase of the amount of charge transfer under pressure toward $(DCNQI^-)_2Cu^{2+}$, a Mott insulator with one electron per each Cu *d* orbital is expected in the insulating phase at high pressures.[121] Then there should exist a metallic region between these two different kinds of Mott insulators, with the incommensurate filling of the π band, which is presumably the one found experimentally. The strong commensurability pinning effect sustains the amount of charge transfer to keep the π band 1/3- and 1/2-filled, and extend their respective insulating regions along the pressure axis. It is theoretically pointed out that this effect is controlled by the interchain Coulomb interaction between *d* and π orbitals, $V_{\pi-d}$.[121] Then, in the members without iodine atom with presumably larger $V_{\pi-d}$ compared to the iodine-contained salt, these two insulators become next to each other and the intermediate metallic phase does not exist, which is shown schematically in Figure 36b.

5.2. Two-Dimensional Systems: ET_2X

The possibility of CO state in 2D ET systems was first suggested theoretically in α-ET_2I_3 by Kino and Fukuyama,[12,123] who treated the Hubbard model, eq 1 with $V = 0$; they found the existence of a slight CD between the two columns along the stacking axis shown in Figure 22 when the value of U is large. The first experimental finding of the CO state in these systems was by Miyagawa et al.[124] using ^{13}C-NMR in another ET compound, θ-$ET_2RbZn(SCN)_4$. The Hubbard model (without V_{ij}) for this compound, however, suggested a DM state due to slight dimerization existing at low temperatures rather than a CO state.[125] Following these, Seo studied the extended Hubbard model with emphasis on the effect of intersite Coulomb interaction, V_{ij}, and found that various CO states can be stabilized in the α-I_3-type structure as well as in the θ-type structure.[126] Then, CO was actually observed in α-ET_2I_3 as well by a ^{13}C-NMR study soon after those works,[127] where the

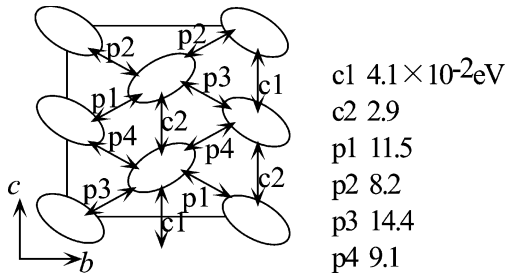

Figure 37. Schematic illustration of the θ_d-type structure.

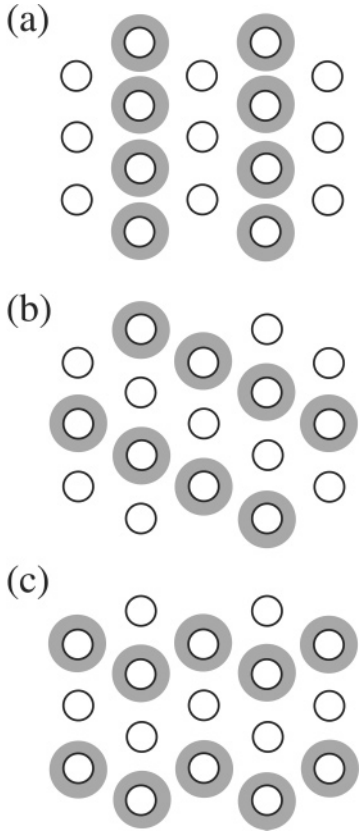

Figure 38. Stripe-type charge ordered states in the (a) vertical, (b) diagonal, and (c) horizontal direction, where "charge-rich" sites are drawn as gray circles.

charge pattern was in accordance with the one suggested by the theoretical considerations.[126]

In these theoretical studies, the anisotropy in the transfer integrals is fully taken into account for each structure shown in Figure 22.[123,126] We note that the θ-type structure turns into a slightly dimerized structure called θ_d-type, as shown in Figure 37, below the structural phase transition accompanied by the MI transition.[47] The MF calculation based on eq 3 to the extended Hubbard model for the θ-type, θ_d-type, and α-I_3-type structures all show the stabilization of CO when the value of intersite Coulomb repulsion V_{ij} is appropriately chosen as $\sim U/4$. In these calculations, two kinds of values for V_{ij} are assumed: the ones along the bonds in the stacking direction, V_c, and those in the inter-stack direction, V_p, which should take similar values judging from the intermolecular distances.[14] Three kinds of CO states with different charge patterns, as shown in Figure 38, are generally found as self-consistent solutions which are called "stripe-type" CO states. These states can be

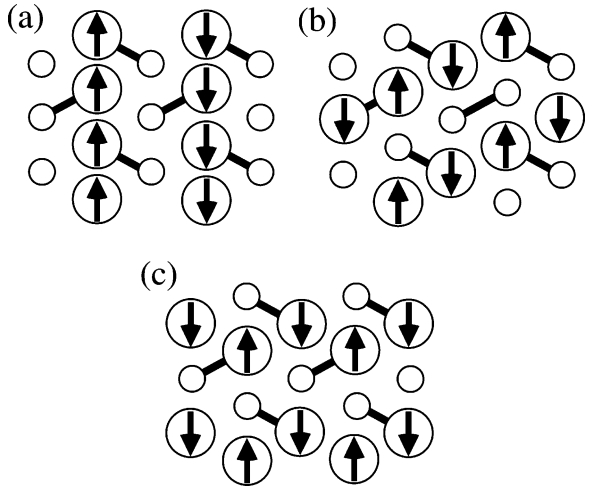

Figure 39. Stripe-type charge ordered states stabilized in θ_d-type structure in the MF calculations where the largest transfer integral t_{p3} is described by thick bonds. The "charge-rich" sites are represented by large circles and the associated spin moment are drawn as arrows. Small spin moments on the "charge-poor" sites are not drawn here (for details see ref 126).

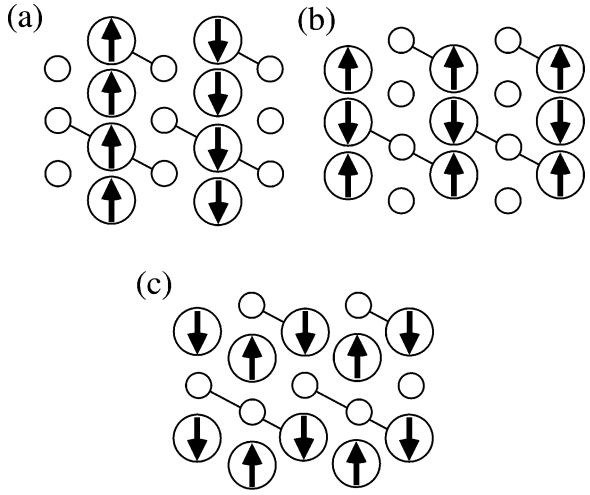

Figure 40. Stripe-type charge ordered states stabilized in α-I_3-type structure in the MF calculations, where the smallest transfer integral t_{p4} is described by thin bonds. The "charge-rich" sites are represented by large circles and the associated spin moment are drawn as arrows. Small spin moments on the "charge-poor" sites are not drawn here (for details see ref 126).

considered as extensions of the Wigner crystal-type CO in 1D systems seen in section 5.1.1 to the 2D triangular lattice systems.

In the case of the θ_d-type structure, stripe-type CO states as shown in Figure 39 are stabilized depending on the relative values of the intersite Coulomb interactions. On the other hand, in the case of α-I_3-type structure, stripe-type CO states as shown in Figure 40 are shown to be stabilized. However, the energies of all these stripe-type CO states in the MF calculation turned out to be very close to each other and sensitive to the value of intersite Coulomb energies as well as to the degree of anisotropy of transfer integrals. Therefore, it is hard to conclude the charge pattern realized in the actual compounds solely from the MF results.

Comparison with the reported magnetic properties of these compounds, where the importance of quantum fluctuation among localized spins are expected, turns out to be a powerful way to decide which charge pattern is actually stabilized. As we have seen in section 5.1.1, the quantum fluctuation can destroy the AF ordering found in MF solutions, and the features of quantum spin systems show up. Since the energy scale of the Coulomb interaction which determines the charge degree of freedom is large compared to the quantum corrections to the spin degree of freedom, the existence of CO is rather robust. This holds even in the 1D systems seen in section 5.1.1, where the quantum fluctuation would affect the ground state properties more seriously than the present 2D systems. Therefore, one can compare the CO patterns stabilized in the MF calculations and the magnetic properties observed in experiments by incorporating the quantum fluctuations expected in the appropriate Heisenberg models. By this procedure, the charge patterns in the insulating phases of both θ-$ET_2RbZn(SCN)_4$ and α-ET_2I_3 are concluded to be the "horizontal stripe-type" one shown in Figures 39c and 40c, respectively, as explained in the following.

The temperature dependences of magnetic susceptibility, χ, are very different between these compounds as mentioned in section 3.3; θ-$ET_2RbZn(SCN)_4$ shows a Bonner−Fisher like curve characteristic of low-dimensional spin system, which varies smoothly through the MI transition temperature,[47] whereas in α-ET_2I_3, a prominent spin gap behavior is observed from just below the MI transition temperature.[72] The magnetic properties of the stripe-type CO states should be described by 1D Heisenberg models with magnetic interaction between localized spins on the "charge-rich" sites along the charge stripes. The effective exchange couplings, J_{ij}, can be estimated from the second-order perturbation as $4t_{ij}^2/(U - V)$ and, therefore, reflect directly the transfer integrals along the stripes. Then, to understand the experimental results above, the CO states are likely to be both the "horizontal stripe-type" for both cases, which has uniform transfer integrals in the θ-type (t_{p4} in Figure 37) and alternating transfer integrals in the α-I_3 type (t_{p2} and t_{p3} in Figure 22), straitforwardly leading to a 1D Heisenberg model with uniform J_{ij} and that with alternating J_{ij}, respectively. We note that there are several possible MF self-consistent solutions with "horizontal stripes" in both structures due to the low symmetry in the unit cell but with higher energy than the ones in Figures 39c and 40c, and so it is important to incorporate the anisotropy for each compound, as has been stressed in section 4.

As a matter of fact, the ^{13}C-NMR experiments in both θ-$ET_2RbZn(SCN)_4$[124,128] and α-ET_2I_3,[127] as well as optical conductivity,[129] Raman scattering,[130,131] and X-ray scattering[132] measurements are consistent with these charge patterns. In the case of θ-$ET_2RbZn(SCN)_4$, the magnetic susceptibility shows a transition at much lower temperature of about 10 K to a spin-gapped state,[47] which is due to the additional instability of the 1D Heisenberg chains of the localized spins along the stripes, i.e., the SP transition.[132]

Since the extended Hubbard models for these 2D CO systems are difficult to treat theoretically beyond MF approximation, works are limited up to now. Merino et al.[133] considered a more simplified model on the square lattice with transfer integrals and intersite Coulomb interaction only for the nearest neighbor sites, where they examined the CO transition with a charge pattern of checkerboard-type, and calculated the optical conductivity.[134] Clay et al.[135] studied a small cluster for the θ-type structure by numerical Lanczos exact diagonalization and discussed a tendency toward bond dimerization under the existence of CO, and its relevance to the structural phase transition observed in θ-$ET_2RbZn(SCN)_4$. Actually, the structural phase transition observed in θ-type compounds (to θ_d-type structure in Figure 37) is speculated[124,126] as due to a cooperative phenomenon between the horizontal stripe-type CO state and the electron−phonon interaction of Peierls-type discussed in section 5.1.2, which needs further theoretical examination.

The pressure effects on the CO state are apparently opposite in the two polytypes of ET_2X, α-I_3-type and θ-type. Namely, the CO transition temperature is suppressed under pressure in α-ET_2I_3,[136] whereas it is enhanced in the θ-type compounds.[47] In α-ET_2I_3, the bandwidth increases with pressure, as usually expected, stabilizing the metallic state over the CO state. As for the θ-type compounds, the decrease in the dihedral angle ϕ is observed under pressure, whose effect is to decrease the bandwidth reflecting the anisotropy of HOMO of ET molecule, contrary to the usual case, explaining the reason of the further stabilization of the CO state. Another effect of pressure here is to decrease the ratio of $|t_c/t_p|$ ($|t/t'|$ in the anisotropic triangular model in Figure 23), which is also seen to work in MF calculations toward the destabilization of the CO.[78] Attempts to control such CO states by uniaxial strain have recently been pursued, where SC states are found in α-ET_2I_3[137] as well as in a θ-type compound but with DIETS molecule different from ET,[138] which will be discussed also in section 8.

Finally, let us discuss the reason CO appears frequently in θ-type compounds and in α-ET_2I_3 but not in the β-type ET compounds and its analogues. As we have pointed out in section 4.3, θ- and α-I_3-types are described as good quarter-filled systems, whereas the β-type is in the crossover region from quarter-filling to half-filling, as concluded from their degree of band splitting. In fact, if the band splitting becomes as large as in β'-$(ET)_2X$, the system becomes effectively half-filled and the DM state instead of CO shows up. Thus, the β-type structure is rather free from both the CO state and the DM state which are favored by quarter-filling and half-filling, respectively. This discussion holds because these molecular solids have the value of V comparable to t, i.e., near the boundary region of having CO or not. In such a case, the degree of anisotropy of transfer integrals becomes an important factor to the stability of the CO state. For example, it is pointed out theoretically that the values of transfer integrals in the θ-ET_2X

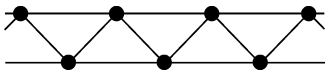

Figure 41. Schematic view of the zigzag ladder structure. Black circles are the lattice sites.

showing CO is actually favorable to the CO state, and the shape of the Fermi surface seems to affect its stability.[78]

Nevertheless, we believe that stripe-type CO is quite ubiquitous in quarter-filled 2D molecular solids (CO in TMTTF compounds can also be viewed as stripes in the 2D TMTTF plane), in cases where the transfer integrals have relatively small values than V. Besides "horizontal stripe"-type CO in the typical family, θ-ET_2X, there are actually other candidates based on different molecules with a quarter-filled band. The "vertical stripes" are inferred in θ-BDT-$TTP_2Cu(NCS)_2$ by optical measurements.[139] Some members of $DODHT_2X$ with β''-type molecular arrangement but with smaller bandwidth than ET compounds show similar behavior with α-ET_2I_3, i.e., MI transition with a spin-gap behavior in χ,[140] which may be due to a similar stripe-type CO. Further studies on compounds based on different molecules will, hence, provide more systematic understanding of the interplay of the value of V and the anisotropy of t_{ij} on the CO state.

5.3. Charge Order under Geometrical Frustration

2D molecular solids frequently have a triangular lattice structure, as has already been pointed out. In such a triangular lattice, the CO state is affected by geometrical frustration. Generally, the geometrical frustration is considered to play an important role in spin systems (see also section 6.1). If one considers lattices where the basic frame is a triangular form and attempts to put spins on the lattice sites in the AF manner coupled to each other, it is impossible to satisfy all bonds with AF alignments; this is the essence of frustration. If one makes correspondence between such spin systems and the CO systems, i.e., up spin and down spin to occupied and unoccupied states, respectively, a similar frustration effect should also be present in the CO systems due to the intersite Coulomb interactions, V_{ij}, on the triangular bonds. This fact was first pointed out by Anderson in the context of a classical CO system, Fe_3O_4, in a three-dimensional frustrated lattice, the pyrochlore lattice.[141]

In the MF calculations on eq 1 explained in the previous section, different stripe patterns have very close energies,[126] namely, the states are nearly degenerate, which is the consequence of such frustration. As a matter of fact, the structural phase transition observed when the CO state emerges in θ-type ET compounds can be considered to be the "effort" of the solid to relax the frustration by lowering the symmetry of the lattice.

However, to treat the effect properly, one needs more elaborated theoretical treatment than the MF level, since quantum fluctuation plays a crucial role. For example, let us discuss a zigzag ladder structure as shown in Figure 41. The extended Hubbard model on this lattice is more easily treated by use of numerical methods than in higher dimensional models such as the triangular lattices, although the essence of the effect of frustration is maintained. Actually, such a structure is realized in the Cu−O subunit of a transition metal oxide $PrBa_2Cu_4O_8$, where a quarter-filled band with fluctuations toward CO is suggested while the resistivity shows a metallic behavior down to the lowest temperature.[142] Numerical calculations suggest that the CO state can be destabilized by the frustration due to the intersite Coulomb interaction, resulting in a metallic state interpreted as "quantum melting" of CO, even when the values of U and V_{ij} remain strong.[143] Whether or not such an effect can be realized in other lattice systems, its possible relevance to the actual compounds, are left for future studies.

6. Dimer-Mott States

The DM insulating state, which is another limiting case of quarter-filling mentioned in section 2.2, has been known from early studies in the 1D A_2B systems.[1] In the presence of strong dimerization, basic features of the electronic properties can be modeled by the half-filled band based on the bonding states (or antibonding states for the 3/4-filling case) of dimers. If the effective Coulomb interaction within a dimer is strong enough, Mott insulators will be realized and this is the DM insulator. The DM state is realized in 1D compounds by the dimerization generated from the electron−phonon interaction, as was mentioned in Sec. 5.1.2, e.g., in MEM-$TCNQ_2$, TEA-$TCNQ_2$, and some members of $DCNQI_2X$ with X = Li, Ag. On the other hand, more recently, it is recognized that there are 2D compounds with strong dimerization originally from the crystal structure, such as κ-ET_2X and λ-$BETS_2X$, which we will explain in this section. For the results of the researches on 1D DM states in the early stage, see ref 1.

6.1. κ-ET_2X

As has already been introduced in section 3.3.3, Kanoda and co-workers constructed a phase diagram shown in Figure 15, on the plane of temperature and pressure (external or chemical) which they interpreted as effective bandwidth, or inversely, effective degree of electron correlation.[57] The interplay of Mott insulator with AF ordering and SC is frequently discussed in comparison with the high-temperature SC copper oxides.[144]

Kino and Fukuyama studied the 3/4-filled Hubbard model (V_{ij} = 0) for the κ-type structure within MF approximation and found that, when U is large an insulating state with AF spin ordering between dimers, as shown in Figure 42, is stabilized in the ground state, which they interpreted as the DM state.[76] They also pointed out that an effective half-filled Hubbard model can describe the electronic properties of κ-ET_2X, which has a triangular lattice structure, as shown in Figure 43. There are two different values of transfer integrals in this model, t and t', and the effective on-site (i.e., "on-dimer") Coulomb interaction, U_{eff}.[12,57,77] These parameters can be estimated from the original quarter-filled model,

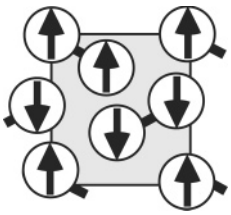

Figure 42. AF between dimers in κ-ET_2X, where the intradimer transfer integral t_A is described by thick bonds. The hole density on each site is 0.5, and the spin order as shown in the Figure is stabilized.

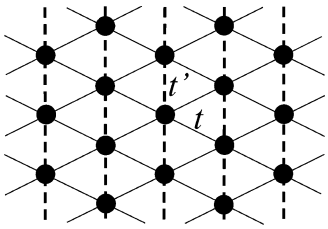

Figure 43. Triangular lattice structure for the dimer model in κ-ET_2X, where the two transfer integrals t and t' are represented by solid and dotted bonds, respectively.

eq 1 with the transfer integrals shown in Figure 22, as $t = t_B/2$, $t' = (t_p - t_q)/2$ (see Table 7), and for $U \gg t$, as $U_{\text{eff}} = 2t + U/2(1 - [1 + (4t/U)^2]^{1/2})$.[12,57] Then it is rather easy to see that, if U_{eff} is large enough, the system will be Mott insulating, and the spin degree of freedom can be described by the $S = 1/2$ Heisenberg spin system on the triangular lattice shown in Figure 43, if t and t' are replaced by exchange couplings, $J = 4t^2/U_{\text{eff}}$ and $J' = 4t'^2/U_{\text{eff}}$, respectively.

After this work, many theoretical studies on the half-filled Hubbard model were applied to κ-ET_2X. For example, dynamical mean field theory was applied to this system to analyze their finite temperature properties.[145] There are several theoretical studies on the SC observed in this family based on the half-filled Hubbard model, which we will see in section 8. Strong coupling approach to map the quarter-filled Hubbard model on the $t-J$ model has also been pursued, and again the DM state is indicated.[146] All of these works point to the fact that the electronic correlation results in the transition from a metallic (or SC) state to a Mott insulator, which is actually discussed in Figure 15.

However, to compare the band structure of each compound and properties summarized in Kanoda's phase diagram more precisely, another parameter more than the effective bandwidth, i.e., the ratio of the transfer integrals between the dimers turned out to be necessary, as was suggested by Hotta.[78,147] It is found that the MI phase boundary is sensitive to the ratio t/t', which controls the density of states near the Fermi level, which has been confirmed in a recent elaborate numerical study.[148] The compounds near the MI boundary in Figure 15 have parameters of the range of $t/t' \sim 0.65-0.8$. The BETS analogue, on the other hand, κ-$BETS_2X$ has smaller U_{eff} and far larger t/t' ($\sim$2) than κ-ET_2X, consistent with the experiments showing metallic behavior for any anions.

Recently, one of these Mott insulating compounds in this family, κ-$ET_2Cu_2(CN)_3$, has been attracting interest, which has almost isotropic transfer integrals as $t/t' \sim 1.05$; this results in the large degree of frustration among localized spins on dimers, $J/J' \sim 1.1$. A spin susceptibility measurement showed that its temperature dependence is well understood by the model of Heisenberg triangular lattice but there has been no indication of any magnetic ordering at least down to 1.9 K,[149] reminiscent of the resonating-valence-bond (RVB) state proposed by Anderson[150] in such a triangular lattice system. Moreover, recent experiment of NMR relaxation rate down to 32 mK indicates that the expected ground state is singlet and the magnetic excitations do not have an energy gap, differently from the RVB idea, i.e., a gapless spin liquid.[149] Theoretical studies on the half-filled Hubbard model to search for such a possibility are under way.[148]

6.2. λ-$BETS_2GaX_4$

As was introduced in section 4.3, λ-$BETS_2GaY_4$ (Y = Cl, Br, etc.) has a strongly dimerized structure coupled in a 2D way. The experimental phase diagram shown in Figure 16a, where the DM insulating phase and the SC phase are located next to each other, has features essentially similar to κ-ET_2X, except the presence of a spin gap in the magnetic susceptibility measurement first reported in the insulating phase.[61] However, a broadening of the ^{1}H NMR spectra toward low temperatures was found and attributed to the emergence of AF moments,[151] although a clear magnetic phase transition with commensurate AF ordering as in κ-ET_2X is not found.

The effective model for this system is considered to be a half-filled Hubbard model as in κ-type compounds. Therefore, analogous phase diagram to κ-ET_2X with the metal (SC)-DM state phase boundary is in fact expected. However, the model for the λ-type structure is rather like a square lattice as shown in Figure 44, where the transfer integrals along the a direction is alternating. Therefore, in the insulating phase, the effective Heisenberg coupling will be alternating, and then the spin gap can be postulated.[152] Actually, the estimation of the Heisenberg coupling constants suggests values quite close to the boundary of quantum phase transition, where the spin gap phase due to the alternation in one direction and the AF phase caused by the 2D coupling along the b-direction compete with each other.[153] The experimental suggestions of the existence of AF without a clear transition may be because the system

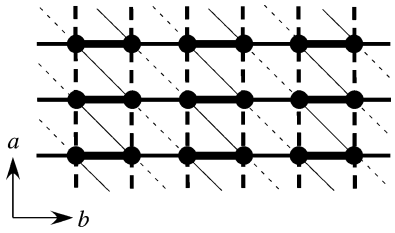

Figure 44. Square lattice model with alternation along the horizontal direction for λ-$BETS_2X$. In the insulating phase, the thicker bonds parallel to the a as well as b axis have larger exchange couplings than the thinner bonds in the diagonal direction, reflecting the values of (effective) transfer integrals between dimers (see Table 7).

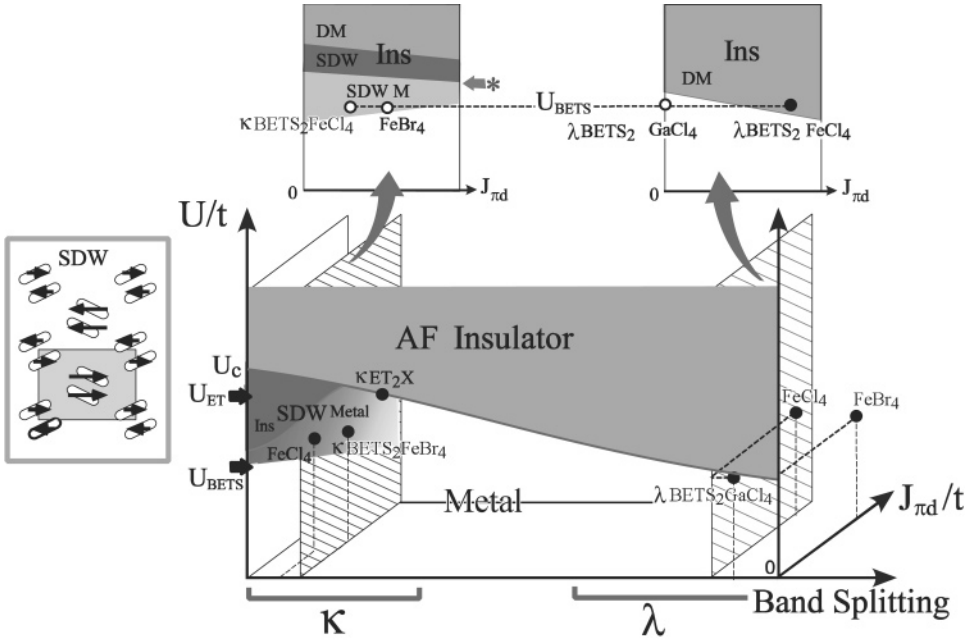

Figure 45. MF phase diagram of the $\pi-d$ system as functions of U, $J_{\pi-d}$, and band splitting in the case of large degree of dimerization. The AF insulating and SDW phases with $J_{\pi-d} \neq 0$ are the DM and SDW states of π electrons, respectively, coexisting with the AF long range ordering of Fe spins. The characteristic spin structure of the SDW state is shown in the inset. In the upper part, the phase diagrams on the plane of U and $J_{\pi-d}$ are shown for two different characteristic values of band splitting which correspond to κ and λ type. The phase boundary indicated by (*) in the left-hand side one is sensitive to the parameter; a downward shift with increasing $J_{\pi-d}$ changes to an upward shift when the degree of band splitting becomes large (in the right-hand side part of the κ-type region).

is near the boundary of these two phases in the AF side, so that the spin moments are reduced by the quantum effect. Another possibility is that the system should be located in the spin gap phase, and the AF moments seen in experiments are those induced by some extrinsic randomness, as observed in several doped transition metal oxides.[154] The competition between the AF state and the spin gap state is also essential in this scenario.[155]

A difference between the κ- and λ-type structures lies in the larger degree of band splitting between the two bands consisting of the antibonding dimer orbitals in the latter, as we have seen in section 4.3. The MF calculations for these two structures suggest that the λ-type structure with larger band splitting requires smaller U to become a Mott insulator than the κ-type one and that the character of the insulating state shows a crossover from the Mott insulator toward the band insulator if one increases the band splitting further.[78] This is consistent with the fact that κ-ET_2X compounds are in the proximity to the Mott transition, whereas κ-$BETS_2X$ with smaller U_{BETS} are always metallic, and on the other hand, λ-$BETS_2X$ show Mott transition as in κ-ET_2X despite $U_{BETS} < U_{ET}$ (see also Figure 45).

It should be noted that, if the materials with far larger band splitting than λ-$BETS_2X$ is realized, the band insulating nature would possibly take place. There are some salts which possibly belong to this band insulating region; the tight-binding calculation of δ'-ET_2GaCl_4, an analogue of the λ-type compounds, shows a clear band gap at the Fermi level and is expected to be such a candidate.[156] λ-ET_2GaI_4[157] and λ-ET_2InBr_4[158] have an insulating character; their relatively narrow bandwidth than BETS-based compounds above and their large degree of band splitting favor the DM state and the band insulator, respectively. The explorations of the magnetic property of these materials is desired to find out which state is realized.

7. Effects of Localized Spins; $\pi-d$ Systems

One of the most fascinating experimental development in recent studies of molecular solids was the successful introduction of the localized moments into the 2D compounds.[159] In such cases, different possibilities from those in purely π-electronic system are expected due to the interaction between these two subsystems. Typical examples are λ- and κ-$BETS_2X$ with $X = FeY_4$ (Y = Cl, Br, etc.), where Fe^{3+} is in the high spin state, $S = 5/2$. Their analogues with $X = GaY_4$ discussed in the previous section, have almost the same band parameters for the π-electron system. The experimental findings imply that the electrons on BETS molecules are interacting with the localized Fe d spins on adjacent 2D planes,[160] whereas the direct magnetic interaction between these spins are weak.[161] The first theoretical consideration on these $\pi-d$ systems was carried out by Brossard et al.[161] on λ-$BETS_2FeCl_4$, who simplified the system as a 2D Kondo-lattice model with a half-filled π band and estimated the RKKY interaction between localized spins when the π band is metallic, where considerations on the "Mott physics" important in this system would be needed as pointed out in refs 162 and 163.

To examine the interplay between the effects of localized d spin and the Coulomb interaction between π electrons (which drives the π system toward DM state as discussed in the previous section), Hotta and

Fukuyama[162] pursued within the MF approximation a more detailed study on the 3/4-filled model with strong dimerization. They took into account all the possible $\pi-d$ interactions, $J_{\pi-d}$, whose values are estimated to be of the order of $\sim 10^{-3}$ eV by use of the data of the extended Hückel calculations. The results can be summarized in the schematic phase diagram shown in Figure 45, where the ground states are shown as functions of U, $J_{\pi-d}$, and the degree of band splitting. The phase diagram at $J_{\pi-d} = 0$ on the plane of U and band splitting is that for the 2D π-electronic system without d spins, where the AF insulating state which is the DM state appears when U exceeds a critical value, U_c. One can see here that the value of U_c is smaller for the λ-type than the κ-type structure, as discussed in section 6.2. We note that in the region of small band splitting relevant to the κ-type compound, another magnetic state is found next to the DM state,[147] which is a SDW state with sinusoidal modulation of small spin moments and cannot be described by the dimer model. Although it is not found experimentally yet, the tendency toward the formation of a density-wave state is suggested.[164]

When $J_{\pi-d}$ is introduced, the AF long range order of d spins takes place in cases where the DM state and the SDW state appear in the π-electronic system, which is the result of the coupling between localized d spins and the π electrons. The DM state is further stabilized by the AF ordering of d spins as seen from two different phase diagrams in Figure 45 on the plane of U and $J_{\pi-d}$. On the other hand, the boundary between the SDW metal and the paramagnetic metal somewhat increases as a function of $J_{\pi-d}$ in the phase diagram for the κ-type structure.

Since the transition between metallic (SC) state and DM state is seen in the experimental phase diagram of λ-$BETS_2GaY_4$ system (Figure 16), these materials are considered to be located around the MI boundary (in Figure 45 the location of $Y = Cl$ for $J_{\pi-d} = 0$ is indicated in the metallic side). Replacement of GaY_4 to FeY_4 corresponds to the introduction of $J_{\pi-d}$. The calculations suggest that in the case of λ-$BETS_2FeY_4$ the d spins order antiferromagnetically with the aid of $J_{\pi-d}$ and then behave as internal local staggered magnetic fields on the π electrons, which, in the case of $Y = Cl$ leads the π electrons toward the DM region from the metallic side where they were at $J_{\pi-d} = 0$. This will be the electronic processes behind the first-order MI transition in λ-$BETS_2FeCl_4$ at 8 K. As for the case of $Y = Br$, the π system alone has an insulating character due to larger degree of band splitting than $Y = Cl$ and $J_{\pi-d}$ does not have large influence on the insulating character itself. On the other hand, the κ-$BETS_2FeY_4$ system is theoretically expected to be in the SDW metal region of the phase diagram (see Figure 45) coexistent with the AF ordering of Fe d spins, which hardly becomes insulating in contrast to the λ-type systems, consistent with the experiments. Even in this case, the small magnetic moments of π electrons partially generated by $J_{\pi-d}$ should possibly exist as predicted in these calculations, although they are not detected yet experimentally.

Another remarkable experimental finding is the novel SC state induced by the external magnetic field, H, applied parallel to the conducting plane as was shown in Figure 17. There, the Fe d spins becomes polarized due to the effect of H, which act as an effective uniform magnetic field due to $J_{\pi-d}$ in the direction opposite to the external field on the π electrons. Then the π electrons experience the addition of these two as an effective field, $H_{eff} = H - \Sigma_i J_{\pi-d}\langle S_i\rangle/g\mu_B$, where $\langle S_i\rangle$, g, and μ_B are the expectation value of the d spin moment on site i, the g-factor, and the Bohr magneton, respectively. When H totally cancels out such effect of $J_{\pi-d}$, i.e., $H_{eff} = 0$, the properties of the π-electron system alone are expected to be reproduced, which are actually the ones in the plane of $J_{\pi-d} = 0$ in Figure 17. Such cancellation is called as Jaccarino-Peter compensation effect.[165] The corresponding experiments in λ-$BETS_2GaY_4$ and κ-$BETS_2GaY_4$ actually shows a SC state for some members, as introduced in sections 3.3.4 and 3.3.3, respectively. This is the explanation of the field-induced SC state, which is discussed more in the next section.

Recently, several materials which involves magnetic ions are found to have other interesting properties; $DMET_2FeBr_4$[166] and $EDTDM_2FeBr_4$[167] which have AF ground states is shown to have a certain degree of π-d interactions, and the latter exhibits negative magnetoresistance under pressure of several GPa. Similar phenomenon is found in quasi-1D conductor $TPP[M(Pc)(CN)_2]_2$ (M = Fe, Co), where only the salts with M = Fe show giant negative magnetoresistance effect.[168] Theoretical explanations to these new phenomena will be necessary.

8. Superconductivity

The first SC in molecular solids was found in 1979 in $TMTSF_2PF_6$,[37] a member of the Bechgaard salts, and more than 100 superconducting materials have been synthesized since then.[2] The SC phase in A_2B compounds frequently exists near an insulating phase, as we have seen in section 3. In such cases, the cause of SC may not be the simple weak coupling BCS mechanism by electron−phonon interaction, but rather due to the electronic correlation. In this section, we review some of those interesting cases. We mention that there are many other SC states not near the insulating phase, such as SC in the β-type compounds found in the early stage of the studies.[2] Many of them are considered implicitly as due to the simple weak coupling BCS mechanism, although the precise nature has not yet been studied both experimentally and theoretically.

8.1. Superconductivity and Magnetism

The SC state in $TMTSF_2PF_6$ and its family is realized next to the SDW phase (see Figure 10),[38] and its nature is believed to be exotic from the initial stage.[169,170] Recently there is a proposal based on experiments that the symmetry of the SC order parameter is a triplet p-wave one,[171] although there still exists controversy.

Similarly, the SC state in κ-ET_2X is also found in the proximity of the magnetic state. Soon after the proposal of Kino and Fukuyama,[12,76] who mainly concerned themselves with possible magnetic ground states, McKenzie[144] noted the potential importance of eq 1 with full anisotropic t_{ij} for the systematic studies including the nature of SC next to magnetic ground states. However, in sharp contrast to the former weak coupling SDW states, this magnetic state is the Mott insulator (strong coupling) with localized spin moment, $S = 1/2$, per dimer,[59] as we have seen in section 6.1. A similar situation is also found in λ-$BETS_2GaX_4$, as has already been discussed in section 6.2. Recently, β'-ET_2IBr_2, an AF insulator with the dimer structure that can be incorporated into Kanoda's phase diagram in the Mott insulating region (see Figure 15), is found to turn into a SC state under pressure as high as ~7GPa.[172]

Such SC next to the Mott insulator may possibly be due to the spin fluctuations. In fact, several theoretical studies from the weak-coupling viewpoint (perturbative approach) have been given on the Hubbard model with the anisotropic triangular lattice structure, mainly by use of the fluctuation exchange (FLEX) approximation.[173] They indicate that the SC mediated by the spin fluctuation favors either the $d_{x^2-y^2}$ or d_{xy} symmetry, whose results are quite sensitive to the band structures,[174] particularly to those near the Fermi level. Experimental confirmation on this issue is now underway.[175]

The competition of AF and SC associated with the Mott transition is one of the most important and interesting topics in solid-state physics but, at the same time, a very difficult one to treat theoretically. The phase diagram of κ-ET_2X in Figure 15 provides a good example on this problem. There exists a critical point at $T = 0$ in the parameter (effective pressure) axis which separates the two characteristic ground states, AF insulator and SC, discontinuously through the first-order transition. From this critical point, a critical line extends toward the finite temperature region eventually ending at some point above both T_N and T_c, as seen in Figure 15, as has been disclosed by recent experiments.[60] The phase diagram of the half-filled Hubbard model computed by the dynamical mean-field theory[176] resembles to the experimental phase diagram, although the SC phase is not reproduced within this theory. There, the existence of an Ising-type order parameter is suggested to characterize the Mott transition, and the boundary between the metallic and Mott insulating phases is described by a gas−liquid phase transition.[177] Onoda and Nagaosa[178] constructed a phenomenological Ginzburg-Landau theory with the order parameters for AF and SC as well as this Ising-type one, and proposed explanations for the experimental phase diagram of κ-ET_2X. Experimentally, however, the critical exponents near the critical end point have been found to differ from the theoretically predicted ones,[179] which are left to be solved.

The field-induced SC in λ-$BETS_2FeY_4$ has a different aspect since it is stabilized only in the presence of the strong magnetic field applied exactly parallel to the 2D π-electron plane. This particular feature is understood in overall within the Jaccarino-Peter compensation mechanism, as explained in section 7, originally applied to *s*-wave SC in metals with large paramagnetic localized moment.[165] Several phenomenological studies have been carried out on the basis of the Jaccarino−Peter mechanism, and the Fulde−Ferrell−Larkin−Ovchinnikov state has been proposed as a cause of the tails of the SC phase on both sides of that characteristic magnetic field.[180] Similar field-induced SC phenomenon predicted in the κ-type analogue[163] has been found in κ-$BETS_2FeBr_4$ very recently.[62] It should be noted that the magnetic $\pi-d$ interaction, $J_{\pi-d}$, is relatively strong and will affect the nature of π-electronic system as mentioned in section 7, whose interplay is not properly taken into account so far, and may bring about another aspect of this SC state. Regarding the symmetry of the order parameters, the precise determination has not been pursued yet, but exotic SC state is naturally expected since the SC state in λ-$BETS_2X$ systems with $X = FeCl_4$ is linked to the SC phase in $X = GaCl_4$[69] as seen in Figure 17, which is next to the DM phase in the phase diagram in Figure 16.

8.2. Superconductivity and Charge Order

Recently, some examples of SC states in the vicinity or in the presence of CO have been reported. α-ET_2I_3 with CO at ambient pressure as we have seen in section 5.2 shows a sharp suppression of resistivity under uniaxial strain which is claimed to be due to SC.[137] If this is the case, this SC appears in the presence of CO as seen in the proposed phase diagram,[137] since the resistivity shows a visible change at some temperature above the SC transition temperature, which shifts continuously from that of CO at ambient pressure.[127] It is noteworthy that the electronic property of the metallic state of α-ET_2I_3 stabilized by high pressure is very peculiar; the temperature dependence of the resistivity is almost flat, and the mobility and carrier number deduced from the transport measurements have very strong temperature dependences.[71] A similar but different competition between SC and CO has been found in a transition metal oxide, β-$Na_{0.33}V_2O_5$, where SC and CO states are exclusive.[181]

θ-$DIETS_2Au(CN)_4$ also shows a sharp suppression of resistivity under uniaxial strain.[138] Since this suppression is sensitive to the external magnetic field, it is considered as due to the onset of SC. The lower pressure side of this phase is an insulating state which is possibly due to the CO state. The value of $t/t' \sim 0.4$ in this compound (see Table 2) is apparently unfavorable for CO as discussed in section 5.2, and then this CO state is presumably due to the small transfer integrals, i.e., large electron correlation. Some $DODHT_2X$ compounds as mentioned previously also have similar features, but controlled with hydrostatic pressure,[140] and then it will be easier to pursue experiments than those under uniaxial pressure.

Possible mechanism for the onset of SC in the proximity to CO phase has been theoretically searched for in the weak coupling approach, ever since Scalapino et al.[182] first studied the extended Hubbard

model in eq 1 on the square lattice with nearest neighbor intersite Coulomb interaction V within random-phase-approximation, suggesting d_{xy} symmetry of the SC order parameter when V is large. Merino et al. studied this model of quarter-filling within the slave-boson approach,[183] and the d_{xy}-SC state was found next to the CO state with a checkerboard pattern. The random-phase-approximation was also applied to the triangular lattice aiming at the SC in θ-type compounds, where it is indicated that when the value of V is appreciable the charge fluctuation rather than the spin fluctuation works in an enhancement of the effective coupling constant of the pairing processes leading to an f-wave symmetry of SC order parameter reflecting the shape of the triangular lattice.[184]

The weak-coupling theories (including the FLEX studies for the κ-ET_2X systems) will apply to the metallic states in the vicinity of the CO (and AF) state and will give some hints to the mechanism and symmetry of superconducting order parameters. However, these approaches cannot be extended into the insulating regions due to strong correlations; therefore, the SC in the presence of CO, if it really exists, will have different and interesting characteristics to be explored.

9. Concluding Remarks

Research activities in conducting molecular solids have been carried out through collaborations between condensed matter physicists and chemists, who used to live in "momentum space" and "real space", respectively. Because of this big difference in scientific cultures, the progress was slow at first. However, after the realization of metallic states in the charge transfer compounds, especially in TTF-TCNQ, there have been strong interests in these new families of materials in the physics community. Because of the particular electronic properties due to one-dimensional crystal structure together with advances in theoretical treatment on one-dimensional systems, there had been great excitements in the early 70's.

Such activities have eventually led to the discovery of superconductivity in 1979 in $TMTSF_2PF_6$, a member of the Bechgaard salts, which is also of charge transfer type but with a different ratio of anions and cations, i.e., 2:1, from former ones with 1:1. The members of this family are generally more metallic than before and then the detailed understanding of the characteristic topology of the Fermi surface of quasi-one-dimensional systems has been achieved by the angular dependent magnetoresistance oscillations (AMRO) studies. The results of these studies are convincing that electrons in molecular solids are just the same as those in traditional metals and semiconductors, but that the electronic states in molecular solids are based on molecular orbitals in contrast to the atomic orbitals. There followed the realization of various two-dimensional systems with this particular anion−cation ratio, whose typical examples are ET_2X and its related families. In this family, various characteristic features of strong correlations have been observed, including Mott insulators and charge ordering together with superconductivity. It is interesting enough that the realization of the Fermi surfaces in molecular solids, namely the characteristic feature of "momentum space", was based on the extended Hückel scheme developed by chemists, whereas the aspects of "real space", Mott insulators and charge ordering, have been introduced to the field mainly by physicists.

The problem of strong correlations is in a word the reconciliation between these "momentum" and "real" spaces. The efforts to understand simultaneously these "momentum" and "real" spaces actually underlies the research history of solids; simple metals, semiconductors, and semimetals, studied from initial stage, are nicely understood based on the Bloch bands, whereas for the understanding of the strongly correlated d and f electrons the features of local atomic orbitals have to be properly taken into account.

Based on these understandings, results of detailed studies on "quarter-filled" A_2B compounds have been reviewed in this paper with special emphasis on the relationship between the band structures and the nature of ground states, to be compared systematically with numerous experimental results. It has been clarified that there exists a competition in these quarter-filled cases between Mott insulators and charge ordering depending on the degree of dimerization and that the charge ordering is a rather usual phenomenon in molecular solids, which is to our surprise not noted earlier at least on a systematic ground. There is a recent experimental indication that superconductivity may be realized in the presence of charge ordering, which, if verified, will also be an interesting problem. In the present review, only either one- or two-dimensional systems have been considered. However, there is another interesting crystal structure, ladders,[185] where interesting phenomena are expected like the charge ordering as in one of the quarter-filled transition metal oxides, NaV_2O_5.[186]

Apart from these fascinating possibilities intrinsic to the π electrons, there are cases where π electrons are interacting with the localized d spins as in the cases of $BETS_2FeY_4$ where the d spins play such particular roles as in the realizations of the field-induced superconductivity. It is expected that there will be many other interesting interplays between π electrons and transition metals in solids, whose understanding could be a basis for the microscopic understandings of electronic properties of biological materials in the future.

10. Acknowledgments

We acknowledge H. Kino, M. Kuwabara, and M. Ogata for collaborations which this review is based on. We are grateful to S. E. Brown, K. Hiraki, R. Kato, A. Kobayashi, H. Kobayashi, K. Miyagawa, H. Mori, T. Mori, T. Takahashi, and many other experimentalists for fruitful discussions over the years, especially K. Kanoda, who also kindly helped us prepare this manuscript. H.S. is supported by Domestic Research Fellowship from Japan Society for the Promotion of Science.

11. References

(1) Farges, J.-P., Ed., *Organic Conductors, Fundamentals and Applications*; Marcel Dekker: New York, 1994.
(2) Ishiguro, T.; Yamaji, K.; Saito, G. *Organic Superconductors*, 2nd ed.; Springer-Verlag: Berlin, 1998.
(3) Bernier, P., Lefrant, S., Bidan, G., Eds.; *Advances in Synthetic Metals, Twenty Years of Progress in Science and Technology*; Elsevier: Amsterdam, 1999.
(4) Recently Kobayashi et al. have succeeded in synthesizing single component molecular crystal realizing metallic state down to low temperatures: Kobayashi, A.; Tanaka, H.; Kobayashi, H. *J. Mater. Chem.* **2001**, *11*, 2078; Kobayashi, A.; Fujiwara, E.; Kobayashi, H. *Chem. Rev.* **2004**, *104*, 5243.
(5) Fukui, K., Fujimoto, H., Eds., *Frontier Orbitals and Reaction Paths: Selected Papers of Kenichi Fukui; World Scientific Series in 20th Century Chemistry, Vol 7*; World Scientific: Singapore, 1997.
(6) Hoffman, R. *J. Chem. Phys.* **1963**, *39*, 1397.
(7) Mori, T.; Kobayashi, A.; Sasaki, T.; Kobayashi, H.; Saito, G.; Inokuchi, H. *Bull. Chem. Soc. Jpn.* **1984**, *57*, 627 and references therein.
(8) Miyazaki, T.; Terakura, K.; Morikawa, Y.; Yamasaki, T. *Phys. Rev. Lett.* **1995**, *74*, 5104.
(9) Miyazaki, T.; Terakura, K. *Phys. Rev. B* **1996**, *54*, 10452.
(10) Uji, S.; Terashima, T.; Aoki, H.; Brooks, J. S.; Kato, R.; Sawa, H.; Aonuma, S.; Tamura, M.; Kinoshita, K. *Phys. Rev. B* **1994**, *50*, 15597.
(11) Kobayashi, A.; Kato, R.; Kobayashi, H.; Mori, T.; Inokuchi, H. *Solid State Comm.* **1987**, *64*, 45.
(12) Kino, H.; Fukuyama, H. *J. Phys. Soc. Jpn.* **1996**, *65*, 2158.
(13) Kato, R.; Kagoshima, S.; Fukuyama, H.; Kino, H.; Seo, H. In ref 3.
(14) Mori, T. *Bull. Chem. Soc. Jpn.* **2000**, *73*, 2243.
(15) Seo, H.; Fukuyama, H. *J. Phys. Soc. Jpn.* **1997**, *66*, 1249.
(16) Fritsch, A.; Ducasse, L. *J. Phys. I* **1991**, *1*, 855. Castet, F.; Fritsch, A.; Ducasse, L. *J. Phys. I France* **1996**, *6*, 583. Ducasse, L.; Fritsch, A.; Castet, F. *Synth. Met.* **1997**, *85*, 1627.
(17) Mila, F. *Phys. Rev. B* **1995**, *52*, 4788.
(18) Devreese, J. T., Evrard, R. P., van Doren, V. E., Eds.; *Highly Conducting One-Dimensional Solids*; Plenum: New York, 1979.
(19) Kagoshima, S., Nagasawa, H., Sambongi, T., Eds.; *One-Dimensional Conductors*; Springer-Verlag: Berlin, 1989.
(20) Epstein, A. J.; Etemad, S.; Garito, A. F.; Heeger, A. J. *Phys. Rev. B* **1972**, *5*, 952.
(21) Pouget, J. P.; Megtert, S.; Comès, R.; Epstein, A. J. *Phys. Rev. B* **1980**, *21*, 486.
(22) Kobayashi, H. *Bull. Chem. Soc. Jpn.* **1975**, *48*, 1373.
(23) Coleman, L. B.; Cohen, M. J.; Sandman, D. J.; Yamagishi, F. G.; Garito, A. F.; Heeger, A. J. *Solid State Comm.* **1973**, *12*, 1125.
(24) Grüner, G. *Density Waves in Solid*; Addison-Wesley: Massachusetts, 1994.
(25) Mori, T.; Inokuchi, H.; Misaki, Y.; Yamabe, T.; Mori, H.; Tanaka, S. *Bull. Chem. Soc. Jpn.* **1994**, *67*, 661.
(26) Mori, T. *Chem. Rev.* **2004**, *104*, 4947 and references therein.
(27) Seo, H.; Kuwabara, M.; Ogata, M. *J. Phys. IV France* **2002**, *12*, Pr9−205.
(28) Ovchinnikov, A. A. *Sov. Phys. JETP* **1973**, *37*, 176. Lee, P. A.; Rice, T. M.; Klemm, R. A. *Phys. Rev. B* **1977**, *15*, 2984. Kondo, J.; Yamaji, K. *J. Phys. Soc. Jpn.* **1978**, *43*, 424. Hubbard, J. *Phys. Rev. B* **1978**, *17*, 494.
(29) Hünig, S.; Herverth, E. *Chem. Rev.* **2004**, *104*, 5535 and references therein.
(30) Hiraki, K.; Kanoda, K. *Phys. Rev. B* **1996**, *54*, 17276.
(31) Aumüller, A.; Erk, P.; Klebe, G.; Hünig, S.; von Schülz, J. U.; Werner, H. P. *Angew. Chem., Int. Ed. Engl.* **1986**, *25*, 740.
(32) Kobayashi, H.; Miyamoto, A.; Kato, R.; Sakai, F.; Kobayashi, A.; Yamakita, Y.; Furukawa, Y.; Tatsumi, M.; Watanabe, T. *Phys. Rev. B* **1993**, *47*, 3500.
(33) Mori, T.; Imaeda, K.; Kato, R.; Kobayashi, A.; Kobayashi, H.; Inokuchi, H. *J. Phys. Soc. Jpn.* **1987**, *56*, 3429. Tomić, S.; Jérome, D.; Aumüller, A.; Erk, P.; Hünig, S.; von Schülz, J. U. *Europhys. Lett.* **1988**, *5*, 553.
(34) Kato, R.; Sawa, H.; Aonuma, S.; Tamura, M.; Kinoshita, M.; Kobayashi, H. *Solid State Comm.* **1993**, *85*, 831. Kato, R.; Aonuma, S.; Sawa, H.; Hiraki, K.; Takahashi, T. *Synth. Met.* **1995**, *68*, 195.
(35) Hiraki, K.; Kobayashi, Y.; Nakamura, T.; Takahashi, T.; Aonuma, S.; Sawa, H.; Kato, R.; Kobayashi, H. *J. Phys. Soc. Jpn.* **1995**, *64*, 2203. Ishida, K.; Kitaoka, Y.; Masuda, H.; Asayama, K.; Takahashi, T.; Kobayashi, A.; Kato, R.; Kobayashi, H. *J. Phys. Soc. Jpn.* **1995**, *64*, 2970. Kawamoto, A.; Miyagawa, K.; Kanoda, K. *Phys. Rev. B* **1998**, *58*, 1243.
(36) Kashimura, Y.; Sawa, H.; Aonuma, S.; Kato, R.; Takahashi, H.; Môri, N. *Solid State Comm.* **1995**, *93*, 675. Kashimura, Y. Thesis, Tokyo University 1998.
(37) Jérome, D.; Mazaud, A.; Ribault, M.; Bechgaard, K. *J. Phys. Lett.* **1980**, *41*, 95.
(38) For reviews, Jérome, D. *Science* **1991**, *252*, 1509. *Physics and Chemistry of Low-Dimensional Inorganic Conductors*; Schlenkler, C., Dumas, J., Greenblatt, M., Van Smaalen, S., Eds.; Plenum Press: New York, 1996; p 141.
(39) Grant, P. M. *J. Phys. (Paris)* **1983**, *44*, C3−847. Ducasse, L.; Abderrabba, M.; Hoarau, J.; Pesquer, M.; Gallois, B.; Gaultier, J. *J. Phys. C* **1986**, *19*, 3805.
(40) Wzietek, P.; Creuzet, F.; Bourbonnais, C.; Jérome, D.; Bechgaard, K.; Batail, P. *J. Phys. I France* **1993**, *3*, 171.
(41) Coulon, C.; Parkin, S. S. P.; Laversanne, R. *Phys. Rev. B* **1985**, *31*, 3583. Javadi, H. H. S.; Laversanne, R.; Epstein, A. J. *Phys. Rev. B* **1988**, *37*, 4280.
(42) Dumm, M.; Loidl, A.; Fravel, B. W.; Starkey, K. P.; Montgomery, L. K.; Dressel, M. *Phys. Rev. B* **2000**, *61*, 511.
(43) Mori, T. *Bull. Chem. Soc. Jpn.* **1998**, *71*, 2509. Mori, T.; Mori, H.; Tanaka, S. *Bull. Chem. Soc. Jpn.* **1999**, *72*, 179. Mori, T. *Bull. Chem. Soc. Jpn.* **1999**, *72*, 2011.
(44) Kato, R.; Kobayashi, H.; Kobayashi, A. *Synth. Met.* **1991**, *41*−*43*, 2093; Kobayashi, A.; Kato, R.; Naito, N.; Kobayashi, H. *Synth. Met.* **1993**, *55*−*57*, 2078.
(45) Takimiya, K.; Jigami, T.; Kawashima, M.; Kodani, M.; Aso, Y.; Otsubo, T. *J. Org. Chem.* **2002**, *67*, 4218.
(46) Kobayashi, H.; Cui, H.; Kobayashi, A. *Chem. Rev.* **2004**, *104*, 5265 and references therein.
(47) Mori, H.; Tanaka, S.; Mori, T. *Phys. Rev. B* **1998**, *57*, 12023.
(48) Mori, H.; Sakurai, N.; Tanaka, S.; Moriyama, H.; Mori, T.; Kobayashi, H.; Kobayashi, A. *Chem. Mater.* **2000**, *12*, 2984. Wang, N. L.; Mori, H.; Tanaka, S.; Dong, J.; Clayman, B. P. *J. Phys. Condens. Matter* **2001**, *13*, 5463.
(49) Parkin, S. S. P.; Engler, E. M.; Schumaker, R. R.; Lagier, R.; Lee, V. Y.; Scott, J. C.; Greene, R. L. *Phys. Rev. Lett.* **1983**, *50*, 270.
(50) Tokumoto, M.; Anzai, H.; Murata, K.; Kajimura, K.; Ishiguro, T. *Jpn J. Appl. Phys.* **1987**, *26*, Suppl. 26-3, 1977.
(51) Hasegawa, Y.; Fukuyama, H. *J. Phys. Soc. Jpn.* **1986**, *55*, 3717.
(52) Mori, T.; Inokuchi, H. *Solid State Commun.* **1987**, *62*, 525.
(53) Emge, T. J.; Wang, H. H.; Leung, P. C. W.; Rust, P. R.; Cook, J. D.; Jackson, P. L.; Carlson, K. D.; Williams, J. M.; Whangbo, M.-H.; Venturini, E. L.; Schirber, J. E.; Azevedo, L. J.; Ferraro, J. R. *J. Am. Chem. Soc.* **1986**, *108*, 695.
(54) Mori, T.; Sasaki, F.; Saito, G.; Inokuchi, H. *Chem. Lett.* **1986**, 1037.
(55) Ugawa, A.; Okawa, Y.; Yakushi, K.; Kuroda, H.; Kawamoto, A.; Tanaka, J.; Tanaka, M.; Nogami, Y.; Kagoshima, S.; Murata, K.; Ishiguro, T. *Synth. Met.* **1988**, *27*, A407.
(56) Ugawa, A.; Yakushi, K.; Kuroda, H.; Kawamoto, A.; Tanaka, J. *Chem. Lett.* **1986**, 1875.
(57) Kanoda, K. *Physica C* **1997**, *282*−*287*, 299; *Hyperfine Int.* **1997**, *104*, 235.
(58) Miyagawa, K.; Kanoda, K. *Chem. Rev.* **2004**, *104*, 5635 and references therein.
(59) Miyagawa, K.; Kawamoto, A.; Nakamura, Y.; Kanoda, K. *Phys. Rev. Lett.* **1995**, *75*, 1174.
(60) Fournier, D.; Poirier, M.; Catonguay, M.; Truong, K. D. *Phys. Rev. Lett.* **2003**, *90*, 127002. Kagawa, F.; Itou, T.; Miyagawa, K.; Kanoda, K. *Phys. Rev. B* **2004**, *69*, 064511.
(61) Tanaka, H.; Ojima, E.; Fujiwara, H.; Nakazawa, Y.; Kobayashi, H.; Kobayashi, A. *J. Mater. Chem.* **2000**, *10*, 245.
(62) Konoike, T.; Nishimura, M.; Yasuzuka, S.; Enomoto, K.; Fujiwara, H.; Zhang, B.; Kobayashi, H.; Uji, S. *Phys. Rev. B* **2004**, *70*, 094514.
(63) Tanaka, H.; Kobayashi, A.; Sato, A.; Akutsu, H.; Kobayashi, H. *J. Am. Chem. Soc.* **1999**, *121*, 760.
(64) Akutsu, H.; Kato, K.; Ojima, E.; Kobayashi, H.; Tanaka, H.; Kobayashi, A.; Cassoux, P. *Phys. Rev. B* **1998**, *58*, 9294.
(65) Sato, A.; Ojima, E.; Kobayashi, H.; Hosokoshi, Y.; Inoue, K.; Kobayashi, A.; Cassoux, P. *Adv. Mater.* **1999**, *14*, 1192.
(66) Tanaka, H.; Adachi, T.; Ojima, E.; Fujiwara, H.; Kato, K.; Kobayashi, H.; Kobayashi, A.; Cassoux, P. *J. Am. Chem. Soc.* **1999**, *121*, 11243.
(67) Tanaka, H.; Kobayashi, H.; Kobayashi, A.; Cassoux, P. *Adv. Mater.* **2000**, *12*, 1685.
(68) Uji, S.; Shinagawa, H.; Terakura, C.; Terashima, T.; Yakabe, T.; Terai, Y.; Tokumoto, M.; Kobayashi, A.; Tanaka, H.; Kobayashi, H. *Nature* **2001**, *410*, 908.
(69) Uji, S.; Terashima, T.; Terakura, C.; Yakabe, T.; Terai, Y.; Yasuzuka, S.; Imanaka, Y.; Tokumoto, M.; Kobayashi, A.; Sakai, F.; Tanaka, H.; Kobayashi, H.; Balicas, L.; Brooks, J. S. *J. Phys. Soc. Jpn.* **2003**, *72*, 369.
(70) Bender, K.; Dietz, K.; Endres, H.; Heiberg, H. W.; Hennig, I.; Keller, H. J.; Schafer, H. W.; Schweitzer, D. *Mol. Cryst. Liq. Cryst.* **1984**, *107*, 84.
(71) Tajima, N.; Tamura, M.; Nishio, Y.; Kajita, K.; Iye, Y. *J. Phys. Soc. Jpn.* **2000**, *69*, 543.
(72) Rothaemel, B.; Forró, L.; Cooper, J. R.; Schilling, J. S.; Weger, M.; Bele, P.; Brunner, H.; Schweizer, D.; Keller, H. J. *Phys. Rev. B* **1986**, *34*, 704.

(73) Singleton, J. *Rep. Prog. Phys.* **2000**, *63*, 1111. Maesato, M.; Kaga, Y.; Kondo, R.; Kagoshima, S. *Phys. Rev. B* **2001**, *64*, 155104. and references therein.
(74) Mori, T.; Kobayashi, A.; Sasaki, Y.; Kobayashi, H. *Chem. Lett.* **1982**, 1923. Whangbo, M.-H.; Walsh, W. M., Jr.; Haddon, R. C.; Wudl, F. *Solid State Commun.* **1982**, *43*, 637. Grant, P. M. *Phys. Rev. B* **1982**, *26*, 6888.
(75) Kino, H.; Fukuyama, H. *J. Phys. Soc. Jpn.* **1995**, *64*, 4523.
(76) Kino, H.; Fukuyama, H. *J. Phys. Soc. Jpn.* **1995**, *64*, 2726.
(77) Okuno, Y.; Fukutome, H. *Solid State Comm.* **1997**, *101*, 355.
(78) Hotta, C. *J. Phys. Soc. Jpn.* **2003**, *72*, 840.
(79) Mori, H.; Tanaka, S.; Mori, T.; Maruyama, Y. *Bull. Chem. Soc. Jpn.* **1995**, *68*, 1136. Mori, T.; Fuse, A.; Mori, H.; Tanaka, S. *Physica C* **1996**, *264*, 22.
(80) Mori, H.; Tanaka, S.; Mori, T.; Kobayashi, A.; Kobayashi, H. *Bull. Chem. Soc. Jpn.* **1998**, *71*, 797.
(81) Komatsu, T.; Sato, H.; Nakamura, T.; Matsukawa, N.; Yamochi, H.; Saito, G.; Kusunoki, M.; Sakaguchi, K.; Kagoshima, S. *Bull. Chem. Soc. Jpn.* **1995**, *68*, 2233.
(82) Mori, H. private communication.
(83) Kobayashi, H.; Kato, R.; Kobayashi, A.; Nishio, Y.; Kajita, K.; Sasaki, W. *Chem. Lett.* **1986**, 789.
(84) Imakubo, T. private communication.
(85) Mori, T.; Kobayashi, A.; Sasaki, Y.; Kobayashi, H.; Saito, G.; Inokuchi, H. *Chem. Lett.* **1984**, 957. Kobayashi, H.; Kato, R.; Kobayashi, A.; Saito, G.; Tokumoto, M.; Anzai, H.; Ishiguro, T. *Chem. Lett.* **1985**, 1293. Kobayashi, H.; Kato, R.; Saito, G.; Tokumoto, M.; Anzai, H.; Ishiguro, T. *Chem. Lett.* **1986**, 89. Mori, T.; Inokuchi, H. *Solid State Comm.* **1987**, *62*, 525. Mori, T.; Sasaki, F.; Saito, G.; Inokuchi, H. *Chem. Lett.* **1986**, 1037.
(86) Geiser, U.; Schultz, H.; Wang, H. H.; Watkins, D. M.; Stupka, D. L.; Williams, J. M.; Schirber, J. E.; Overmyer, D. L.; Jung, D.; Novoa, J. J.; Whangbo, M.-H. *Physica C* **1991**, *174*, 475. Mori, T.; Mori, H.; Tanaka, S. *Bull. Chem. Soc. Jpn.* **1999**, *72*, 179.
(87) Watanabe, M.; Nogami, Y.; Oshima, K.; Ito, H.; Ishiguro, T.; Saito, G. *Synth. Met.* **2999**, *103*, 1909.
(88) Oshima, K.; Mori, T.; Inokuchi, H.; Urayama, H.; Yamochi, H.; Saito, G. *Phys. Rev. B* **1988**, *38*, 938. Kobayashi, A.; Kato, R.; Kobayashi, H.; Moriyama, S.; Nishio, Y.; Kajita, K.; Sadaki, W. *Chem. Lett.* **1987**, 459.
(89) Kobayashi, A. private communications.
(90) Mori, H.; Tanaka, S.; Oshima, M.; Saito, G.; Mori, T.; Maruyama, Y.; Inokuchi, H. *Bull. Chem. Soc. Jpn.* **1990**, *63*, 2183.
(91) Mori, T.; Kobayashi, A.; Sasaki, Y.; Kobayashi, H.; Saito, G.; Inokuchi, H. *Chem. Lett.* **1984**, 957.
(92) Hiraki, K.; Kanoda, K. *Phys. Rev. Lett.* **1998**, *80*, 4737.
(93) Mila, F.; Zotos, X. *Europhys. Lett.* **1993**, *24*, 133.
(94) Penc, K.; Mila, F. *Phys. Rev. B* **1994**, *49*, 9670. Sano, K.; Ōno, Y. *J. Phys. Soc. Jpn.* **1994**, *63*, 1250. Nakamura, M. *Phys. Rev. B* **2000**, *61*, 16377.
(95) Penc, K.; Mila, F. *Phys. Rev. B* **1994**, *50*, 11429.
(96) Shibata, Y.; Nishimoto, S.; Ohta, Y. *Phys. Rev. B* **2001**, *64*, 235107.
(97) Yoshioka, H.; Tsuchiizu, M.; Suzumura, Y. *J. Phys. Soc. Jpn.* **2000**, *69*, 651; *J. Phys. Soc. Jpn.* **2001**, *70*, 762.
(98) Tsuchiizu, M.; Yoshioka, H.; Suzumura, Y. *J. Phys. Soc. Jpn.* **2001**, *70*, 1460.
(99) Fukuyama, H.; Takayama, H. In *Electronic Properties of Inorganic Quasi-One-Dimensional Compounds*; Monceau, P., Ed.; D. Reidel Publishing Company, Dordrecht, The Netherlands, 1985; p 41.
(100) Emery, V. J.; Bruisma, R.; Barišić, S. *Phys. Rev. Lett.* **1982**, *48*, 1039.
(101) Giamarchi, T. *Physica B* **1997**, *230*−*232*, 975. Yonemitsu, K. *Phys. Rev. B* **1997**, *56*, 7262.
(102) Itou, T.; Kanoda, K.; Murata, K.; Matsumoto, T.; Hiraki, K.; Takahashi, T. preprint.
(103) Nogami, Y.; Oshima, K.; Hiraki, K.; Kanoda, K. *J. Phys. IV* **1999**, *9*, Pr10−357.
(104) Nakamura, T.; Nobutoki, T.; Kobayashi, Y.; Takahashi, T.; Saito, G. *Synth. Met.* **1995**, *70*, 1293.
(105) Chow, D. S.; Zamborsky, F.; Alavi, B.; Tantillo, D. J.; Baur, A.; Merlic, C. A.; Brown, S. E. *Phys. Rev. Lett.* **2000**, *85*, 1698.
(106) Nad, F.; Monceau, P.; Fabre, J. M. *Phys. Rev. B* **2000**, *62*, 1753; *J. Phys. Cond. Matter* **2000**, *12*, L435. Monceau, P.; Nad, F. Ya.; Brasovskii, S. *Phys. Rev. Lett.* **2001**, *86*, 4080.
(107) Zamborzky, F.; Yu, W.; Raas, W.; Brown, S. E.; Alavi, B.; Merlic, C. A.; Baur, A. *Phys. Rev. B* **2002**, *66*, 081103.
(108) Yu, W.; Zamborszky, F.; Alavi, B.; Baur, A.; Merlic, C. A.; Brown, S. E. *Phys. Rev. B* **2004**, *70*, 121101.
(109) Inagaki, S.; Fukuyama, H. *J. Phys. Soc. Jpn.* **1983**, *52*, 3620. Fukuyama, H.; Inagaki, S. In *Magnetic Properties of Low-Dimensional Systems*; Falikov, L. M., Morán-López, J. L., Eds.; Springer-Verlag: Berlin, 1986; p 156.
(110) Kishine, J.; Yonemitsu, K. *Int. J. Mod. Phys. B* **2002**, *16*, 711, and references therein.
(111) Kuwabara, M.; Seo, H.; Ogata, M. *J. Phys. Soc. Jpn.* **2003**, *72*, 225.
(112) Huizinga, S.; Kommandeur, J.; Sawatzky, G. A.; Thole, B. T.; Kopinga, K.; de Jonge, W. J. M.; Roos, J. *Phys. Rev. B* **1979**, *19*, 4723. Ung, K. C.; Mazumdar, S.; Toussaint, D. *Phys. Rev. Lett.* **1994**, *73*, 2603. Riera, J.; Poilblanc, D. *Phys. Rev. B* **2000**, *62*, 16243.
(113) For example, see: Clay, R. T.; Mazumdar, S.; Campbell, D. K. *Phys. Rev. B* **2003**, *67*, 115121.
(114) Riera, J.; Poilblanc, D. *Phys. Rev. B* **2001**, *63*, 241102.
(115) Inoue, I. H.; Kakizaki, A.; Mamatame, H.; Fujimori, A.; Kobayashi, A.; Kato, R.; Kobayashi, H. *Phys. Rev.* **1992**, *B45*, 5828.
(116) Kawamoto, A.; Miyagawa, K.; Kanoda, K. *Phys. Rev. Lett.* **2001**, *87*, 106602.
(117) Fukuyama, H. *J. Phys. Soc. Jpn.* **1992**, *61*, 3452. Suzumura, Y.; Fukuyama, H. *J. Phys. Soc. Jpn.* **1992**, *61*, 3322.
(118) Nakano, M.; Kato, M.; Yamada, K. *Physica B* **1993**, *186*−*188*, 1077.
(119) Nishio, Y.; Tamura, M.; Kajita, K.; Aonuma, S.; Sawa, H.; Kato, R.; Kobayashi, H. *J. Phys. Soc. Jpn.* **2000**, *69*, 1414.
(120) Ogawa, T.; Suzumura, Y. *J. Phys. Soc. Jpn.* **1994**, *63*, 2066; *Phys. Rev. B* **1995**, *51*, 10293.
(121) Hotta, C.; Fukuyama, H. *J. Phys. Soc. Jpn.* **1999**, *68*, 941; Hotta, C. *J. Phys. Soc. Jpn.* **1999**, *68*, 2703.
(122) Miyazaki, T.; Terakura, K. *Phys. Rev. B* **1997**, *56*, 477.
(123) Kino, H.; Fukuyama, H. *J. Phys. Soc. Jpn.* **1995**, *64*, 1877.
(124) Miyagawa, K.; Kawamoto, A.; Kanoda, K. *Phys. Rev. B* **2000**, *62*, 7679.
(125) Seo, H.; Fukuyama, H. *J. Phys. Soc. Jpn.* **1998**, *67*, 1848.
(126) Seo, H. *J. Phys. Soc. Jpn.* **2000**, *69*, 805.
(127) Takano, Y.; Hiraki, K.; Yamamoto, H. M.; Nakamura, T.; Takahashi, T. *J. Phys. Chem. Solid* **2001**, *62*, 393.
(128) Chiba, R.; Yamamoto, H. M.; Nakamura, T.; Takahashi, T. *J. Phys. Chem. Solids* **2001**, *62*, 389.
(129) Tajima, H.; Kyoden, S.; Mori, H.; Tanaka, S. *Phys. Rev. B* **2000**, *62*, 9378.
(130) Yamamoto, K.; Yakushi, K.; Miyagawa, K.; Kanoda, K.; Kawamoto, A. *Phys. Rev. B* **2002**, *65*, 085110.
(131) Wojciechowski, R.; Yamamoto, K.; Yakushi, K.; Inokuchi, M.; Kawamoto, A. *Phys. Rev. B* **2003**, *67*, 224105.
(132) Watanabe, M.; Noda, Y.; Nogami, Y.; Mori, H. *J. Phys. Soc. Jpn.* **2004**, *73*, 116.
(133) Calandra, M.; Merino, J.; McKenzie, R. H. *Phys. Rev. B* **2002**, *66*, 195102.
(134) Merino, J.; Greco, A.; McKenzie, R. H.; Calandra, M. *Phys. Rev. B* **2003**, *68*, 245121.
(135) Clay, R. T.; Mazumdar, S.; Campbell, D. K. *J. Phys. Soc. Jpn.* **2002**, *71*, 1816.
(136) Schwenk, H.; Cross, F.; Heidmann, C. P.; Andres, K.; Schweitzer, D.; Keller, H. *Mol. Cryst. Liq. Cryst.* **1985**, *119*, 329.
(137) Tajima, N.; E-Tajima, A.; Tamura, M.; Nishio, Y.; Kajita, K. *J. Phys. Soc. Jpn.* **2002**, *71*, 1832.
(138) Tajima, N.; Imakubo, T.; Kato, R.; Nishio, Y.; Kajita, K. *J. Phys. Soc. Jpn.* **2003**, *72*, 1014.
(139) Ouyang, J.; Yakushi, K.; Misaki, Y.; Tanaka, K. *Phys. Rev. B* **2001**, *63*, 054301. Yakushi, K.; Yamamoto, K.; Simonyan, M.; Ouyang, J.; Nakano, C.; Misaki, Y.; Tanaka, K. *Phys. Rev. B* **2002**, *66*, 235102.
(140) Nishikawa, H.; Morimoto, T.; Kodama, T.; Ikemoto, I.; Kikuchi, K.; Yamada, J.; Yoshino, H.; Murata, K. *J. Am. Chem. Soc.* **2002**, *124*, 730. Nishikawa, H.; Machida, A.; Morimoto, T.; Kikuchi, K.; Kodama, T.; Ikemoto, I.; Yamada J, J.; Yoshino, H.; Murata, K. *Chem. Commun.* **2003**, 494.
(141) Anderson, P. W. *Phys. Rev.* **1956**, *102*, 1008.
(142) Fujiyama, S.; Takigawa, M.; Horii, S. *Phys. Rev. Lett.* **2003**, *90*, 147004, and references therein.
(143) Seo, H.; Ogata, M. *Phys. Rev. B* **2001**, *64*, 113103; *Phys. Rev. B* **2002**, *65*, 169902(E). Nishimoto, S.; Ohta, Y. *Phys. Rev. B* **2003**, *68*, 235114.
(144) McKenzie, R. H. *Science* **1997**, *278*, 820; *Comments Cond. Mater. Phys.* **1998**, *18*, 309.
(145) Merino, J.; McKenzie, R. H. *Phys. Rev. B* **2001**, *61*, 7996.
(146) Nishimoto, S.; Ohta, Y. *J. Phys. Soc. Jpn.* **1998**, *67*, 2598.
(147) Hotta, C.; Fukuyama, H. *J. Phys. Soc. Jpn.* **2001**, *70*, 321.
(148) Morita, H.; Watanabe, S.; Imada, M. *J. Phys. Soc. Jpn.* **2001**, *71*, 2109.
(149) Shimizu, Y.; Miyagawa, K.; Kanoda, K.; Maesato, M.; Saito, G. *Phys. Rev. Lett.* **2003**, *91*, 107001.
(150) Anderson, P. W. *Mater. Res. Bull.* **1973**, *8*, 153.
(151) Miyagawa, K.; Kanoda, K. private communications.
(152) Seo, H.; Fukuyama, H. *J. Phys. Soc. Jpn.* **1997**, *66*, 3352.
(153) Katoh, N.; Imada, M. *J. Phys. Soc. Jpn.* **1994**, *63*, 4529.
(154) Uchinokura, K. *J. Phys. Condens. Matter* **2002**, *14*, R195.
(155) Fukuyama, H.; Tanimoto, T.; Saito, M. *J. Phys. Soc. Jpn.* **1996**, *65*, 1182; Saito, M. *J. Phys. Soc. Jpn.* **1998**, *67*, 2477; *J. Phys. Soc. Jpn.* **1999**, *68*, 2898.
(156) Mori, H.; Kamiya, M.; Haemori, M.; Suzuki, H.; Tanaka, S.; Nishio, Y.; Kajita, K.; Moriyama, H. *J. Am. Chem. Soc.* **2002**, *124*, 1251.

(157) Geiser, U.; Wang, H. H.; Schlueter, J. S.; Hallenbeck, S. L.; Allen, T. A.; Chen, M. Y.; Kao, H.-C. I.; Carlson, K. D.; Gerdom, L. E.; Williams, J. M. *Acta Crystallogr.* **1988**, *C44*, 1544.
(158) Beno, M. A.; Cox, D. D.; Williams, J. M.; Kwak, J. F. *Acta Crystallogr.* **1984**, *C40*, 1334.
(159) Day, P.; Coronado, E. *Chem. Rev.* **2004**, *104*, 5419 and references therein.
(160) Kobayashi, H.; Tomita, H.; Naito, T.; Kobayashi, A.; Sakai, F.; Watanabe, T.; Cassoux, P. *J. Am. Chem. Soc.* **1996**, *118*, 368.
(161) Brossard, L.; Clerac, R.; Coulon, C.; Tokumoto, M.; Ziman, T.; Petrov, D. K.; Laukhin, V. N.; Naughton, M. J.; Audouard, A.; Goze, F.; Kobayashi, A.; Cassoux, P. *Eur. Phys. J. B* **1998**, *1*, 439.
(162) Hotta, C.; Fukuyama, H. *J. Phys. Soc. Jpn.* **2000**, *69*, 2577.
(163) Cepas, O.; McKenzie, R.; Merino, J. *Phys. Rev. B* **2002**, *65*, 100502.
(164) Tanatar, M. A.; Kagoshima, S.; Ishiguro, T.; Ito, H.; Yefanov, V. S.; Bondarenko, V. A.; Kushch, N. D.; Yagubskii, E. B. *Phys. Rev. B* **2000**, *62*, 15561.
(165) Jaccarino, V.; Peter, M. *Phys. Rev. Lett.* **1962**, *9*, 290.
(166) Enomoto, K.; Yamaura, J.-I.; Miyazaki, A.; Enoki, T. *Bull. Chem. Soc. Jpn.* **2003**, *76*, 945.
(167) Okabe, K.; Miyazaki, A.; Enoki, T. *Synth. Met.* **2003**, *135*−*136*, 693.
(168) Hanasaki, N.; Tajima, H.; Matsuda, M.; Naito, T.; Inabe, T. *Phys. Rev. B* **2000**, *62*, 5839.
(169) Takigawa, M.; Yasuoka, H.; Saito, G. *J. Phys. Soc. Jpn.* **1987**, *56*, 873.
(170) Hasegawa, Y.; Fukuyama, H. *J. Phys. Soc. Jpn.* **1987**, *56*, 877.
(171) Lee, I. J.; Brown, S. E.; Clark, W. G.; Strouse, M. J.; Naughton, M. J.; Kang, W.; Chaikin, P. M. *Phys. Rev. Lett.* **2002**, *88*, 017004.
(172) Taniguchi, H.; Miyashita, M.; Uchiyama, K.; Satoh, K.; Mori, N.; Okamoto, H.; Miyagawa, K.; Kanoda, K.; Hedo, M.; Uwatoko, Y. *J. Phys. Soc. Jpn.* **2003**, *72*, 468.
(173) Kino, H.; Kontani, H. *J. Phys. Soc. Jpn.* **1998**, *67*, 3691. Schmalian, J.; *Phys. Rev. Lett.* **1998**, *81*, 4232. Kondo, H.; Moriya, T. *J. Phys. Soc. Jpn.* **1998**, *67*, 3695. Kondo, H.; Moriya, T. *J. Phys. C.* **1999**, *11*, L363. Kuroki, K.; Aoki, H. *Phys. Rev. B* **1999**, *60*, 3060. Kontani, H. *Phys. Rev. B* **2003**, *67*, 180503.
(174) Kuroki, K.; Kimura, T.; Arita, R.; Tanaka, Y.; Matsuda, Y. *Phys. Rev. B* **2002**, *65*, 100516.
(175) See, e.g.: Arai, T.; Ichimura, K.; Nomura, K.; Takasaki, S.; Yamada, J.; Nakatsuji, S.; Anzai, H. *Phys. Rev. B* **2001**, *63*, 104518. Izawa, K.; Yamaguchi, H.; Sasaki, T.; Matsuda, Y. *Phys. Rev. Lett.* **2002**, *88*, 027002, and references therein.
(176) Rozenberg, M. J.; Kotliar, G.; Zhang, X. Y. *Phys. Rev. B* **1994**, *49*, 10181. Georges, A.; Kotliar, G.; Krauth, W.; Rozenberg, M. J. *Rev. Mod. Phys.* **1996**, *68*, 13.
(177) Kotliar, G.; Lange, E.; Rozenberg, M. J. *Phys. Rev. Lett.* **2000**, *84*, 5180.
(178) Onoda, S.; Nagaosa, N. *J. Phys. Soc. Jpn.* **2003**, *72*, 2445.
(179) Kagawa, F.; Itou, T.; Miyagawa, K.; Kanoda, K. private communications.
(180) Shimahara, H. *J. Phys. Soc. Jpn.* **2002**, *71*, 1644. Houzet, M.; Buzdin, A.; Bulaevskii, L.; Maley, M. *Phys. Rev. Lett.* **2002**, *88*, 227001.
(181) Yamauchi, T.; Ueda, Y.; Môri, N. *Phys. Rev. Lett.* **2002**, *89*, 057002.
(182) Scalapino, D. J.; Loh, E., Jr.; Hirsch, J. E. *Phys. Rev. B* **1987**, *35*, 6694.
(183) Merino, J.; McKenzie, R. H. *Phys. Rev. Lett.* **2001**, *87*, 237002.
(184) Tanaka, Y.; Yanase, Y.; Ogata, M. *J. Phys. Soc. Jpn* **2004**, *73*, 319.
(185) Rovira, C. *Chem. Eur. J.* **2000**, *6*, 1723.
(186) Isobe, M.; Ueda, Y. *J. Phys. Soc. Jpn.* **1996**, *65*, 1178. Seo, H.; Fukuyama, H. *J. Phys. Soc. Jpn.* **1998**, *67*, 2602.

CR030646K